The gut–brain axis mediates sugar preference

https://doi.org/10.1038/s41586-020-2199-7

Received: 12 April 2019

Accepted: 21 February 2020

Published online: 15 April 2020

Check for updates

Hwei-Ee Tan[1,2,4], Alexander C. Sisti[1,3,4], Hao Jin[1,3], Martin Vignovich[1,3], Miguel Villavicencio[1,3], Katherine S. Tsang[1,3], Yossef Goffer[3] & Charles S. Zuker[1,3]✉

The taste of sugar is one of the most basic sensory percepts for humans and other animals. Animals can develop a strong preference for sugar even if they lack sweet taste receptors, indicating a mechanism independent of taste[1–3]. Here we examined the neural basis for sugar preference and demonstrate that a population of neurons in the vagal ganglia and brainstem are activated via the gut–brain axis to create preference for sugar. These neurons are stimulated in response to sugar but not artificial sweeteners, and are activated by direct delivery of sugar to the gut. Using functional imaging we monitored activity of the gut–brain axis, and identified the vagal neurons activated by intestinal delivery of glucose. Next, we engineered mice in which synaptic activity in this gut-to-brain circuit was genetically silenced, and prevented the development of behavioural preference for sugar. Moreover, we show that co-opting this circuit by chemogenetic activation can create preferences to otherwise less-preferred stimuli. Together, these findings reveal a gut-to-brain post-ingestive sugar-sensing pathway critical for the development of sugar preference. In addition, they explain the neural basis for differences in the behavioural effects of sweeteners versus sugar, and uncover an essential circuit underlying the highly appetitive effects of sugar.

Sugar is a fundamental source of energy for all animals, and correspondingly, most species have evolved dedicated brain circuits to seek, recognize and motivate its consumption[4]. In humans, the recruitment of these circuits for reward and pleasure—rather than nutritional needs—is thought to be an important contributor to the overconsumption of sugar and the concomitant increase in obesity rates. In the 1800s the average American consumed less than 4.5 kg of sugar per year[5]; today, following the broad availability of refined sugar in consumer products, the average consumption is more than 45 kg per year[6].

Sweet compounds are detected by specific taste receptor cells on the tongue and palate epithelium[7,8]. Activation of sweet taste receptor cells sends hardwired signals to the brain to elicit recognition of sweet-tasting compounds[9,10]. We and others have studied the circuits linking activation of sweet taste receptors on the tongue to sweet-evoked attraction[8,11,12]. Surprisingly, even in the absence of a functional sweet-taste pathway, animals can still acquire a preference for sugar[1,2,7]. Furthermore, although artificial sweeteners activate the same sweet taste receptor as sugars, and they may do so with vastly higher affinities[7], they fail to substitute for sugar in generating a behavioural preference[13].

Together, these results suggested the existence of a sugar-specific, rather than sweet-taste-specific pathway, that operates independently of the sense of taste to create preference for sugar and motivate consumption[2,14]. Here, we dissect the neural basis for sugar preference.

Sweet versus sugar preference

When non-thirsty, wild-type mice are given a choice between water and sugar they drink almost exclusively from the sugar solution[7]. If, however, they are allowed to choose between an artificial sweetener (for example, acesulfame K (AceK)) and sugar, using concentrations at which both are equally attractive, naive mice initially drink from both bottles at a similar rate (Fig. 1a). However, within 24 h of exposure to both choices, their preference is markedly altered, such that by 48 h, they drink almost exclusively from the bottle containing sugar (Fig. 1a, b, compare 15 h with 48 h). This behavioural switch also happens in knockout (KO) mice lacking sweet taste (*Trpm5*$^{-/-}$ (hereafter TRPM5 KO)[15,16] or *Tas1r2*$^{-/-}$*Tas1r3*$^{-/-}$ (hereafter T1R2/3 KO)[7]; Fig. 1c). Similar observations have been made in several studies, primarily using flavour-conditioning assays[1,2]. Thus, although taste-knockout mice cannot taste sugar or sweetener, they learn to recognize and choose the sugar, most probably as a result of strong positive post-ingestive effects[17].

Notably, the preference for sugar does not rely on its caloric content[18]. For example, if sugar is substituted for the non-metabolizable glucose analogue (methyl-α-D-glucopyranoside (MDG))[19] mice still develop a strong preference for MDG, just as they do for glucose (Fig. 1b; Extended Data Fig. 1). Thus, the signalling system recognizes the sugar molecule itself rather than its caloric content or metabolic products.

[1]Zuckerman Mind Brain Behavior Institute, Howard Hughes Medical Institute and Department of Biochemistry and Molecular Biophysics, Columbia University, New York, NY, USA. [2]Department of Biological Sciences, Columbia University, New York, NY, USA. [3]Department of Neuroscience, Vagelos College of Physicians and Surgeons, Columbia University, New York, NY, USA. [4]These authors contributed equally: Hwei-Ee Tan, Alexander C. Sisti. ✉e-mail: cz2195@columbia.edu

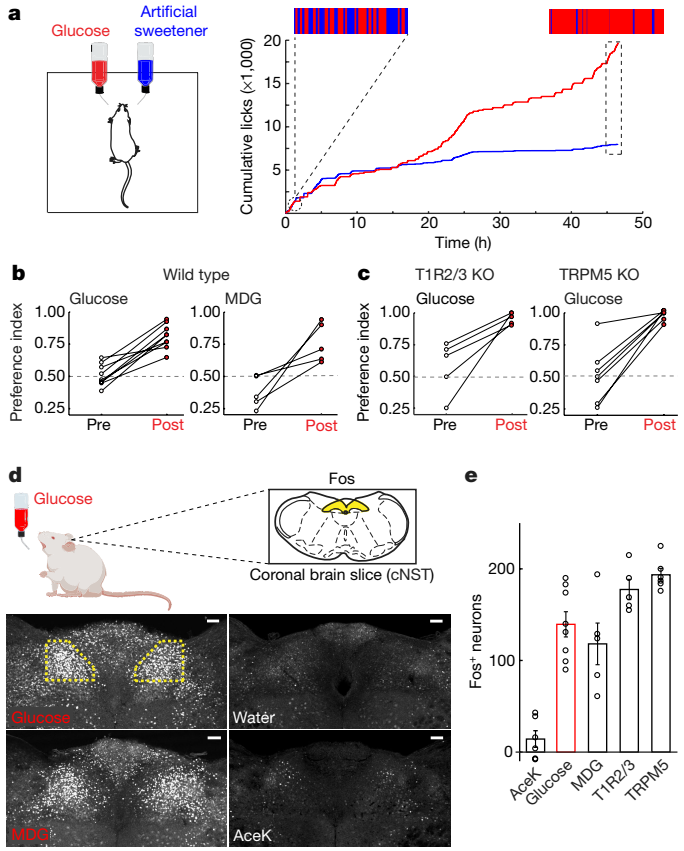

Fig. 1 | Sugar activates the gut–brain axis. a, Mice were allowed to choose between 600 mM glucose and 30 mM AceK (sweetener). Preference was tracked by electronic lick counters in each port. Bars at the top show lick rasters for glucose (red) versus AceK (blue) from the first and last 2,000 licks of the behavioural test. Note that by 48 h the animals drink almost exclusively from the sugar bottle. **b**, Preference plots for sugar versus AceK ($n = 9$ mice, two-tailed paired t-test, $P = 2.39 \times 10^{-6}$) and MDG versus AceK ($n = 5$ mice, two-tailed paired t-test, $P = 0.0024$; Extended Data Fig. 1). Note that mice may begin the behavioural preference test exhibiting no preference for sugar (preference index ≈ 0.5), some preference for sugar (preference index > 0.5) or with an initial preference for the sweetener (preference index < 0.5). However, in all cases they switched (or substantially increased) their preference towards sugar. **c**, Mice lacking the sweet taste receptor (T1R2/3 KO)[7] ($n = 5$ mice, two-tailed paired t-test, $P = 0.0038$), and mice lacking TRPM5 (TRPM5 KO)[15] ($n = 7$ mice, two-tailed paired t-test, $P = 0.0001$) switched their preference to sugar even though they cannot taste it. **d**, Schematic of sugar stimulation of Fos induction. Strong Fos labelling is observed in neurons of the cNST (highlighted yellow). Scale bars, 100 µm. Similar results were obtained in multiple mice in each experiment (Extended Data Fig. 2). **e**, Quantification of Fos-positive neurons. The equivalent area of the cNST (bregma −7.5 mm) was processed and counted for the different stimuli. The signal present in water alone was subtracted before plotting; ANOVA with Tukey's honestly significant difference (HSD) post hoc test against AceK ($n = 6$ mice): $P = 4.68 \times 10^{-5}$ (glucose, $n = 8$ mice), $P = 0.001$ (MDG, $n = 5$ mice). Values are mean ± s.e.m.

Brain neurons activated by sugar

For an animal to develop a preference for sugar over sweetener, it must recognize and distinguish between two innately attractive stimuli. We reasoned that if we could identify a population of neurons that respond selectively to the consumption of sugar, it may provide an entry to reveal the neural control of sugar preference and the basis of sugar craving.

We exposed separate cohorts of mice to sugar, sweetener or water, and examined their brains for induction of Fos as a proxy for neural activity[20] (see Methods). Our results showed prominent bilateral labelling in the caudal nucleus of the solitary tract (cNST; Fig. 1d), an area known to function as a nexus of interoceptive signals conveying information from the body to the brain[21]. By contrast, the cNST was not substantially labelled in response to sweetener or water controls (Fig. 1d, Extended Data Fig. 2a). Furthermore, if these cNST neurons are involved in sugar-preference behaviour, they must also be activated by MDG (Fig. 1d, e), and their activation by sugar should be independent of the taste system (Extended Data Fig. 3a).

How do sugar signals reach the cNST? The finding that preference for sugar does not require the taste system strongly suggested post-ingestive recognition. Therefore, we tested whether intragastric application of sugar was sufficient to activate the cNST. As predicted, direct gut infusion of sugar (but not sweetener) is sufficient to activate the cNST as robustly as oral ingestion (Extended Data Fig. 3b). These results also substantiate previous behavioural studies showing that intragastric infusion of glucose is sufficient to condition flavour preference[22,23].

The gut–brain axis

A number of recent studies have implicated the gut–brain axis as a key mechanism for transmitting information from the gut to the brain via the vagus nerve[24–26]. The gut–brain axis is emerging as a fundamental conduit for the transfer of neural signals informing the brain of the metabolic and physiologic state of the body. If information about sugar detection is being transferred from the gut to the cNST via the gut–brain axis, then it should be possible to directly monitor the activity of this circuit by using real-time recordings of cNST activation in response to synchronized gut stimulation with sugar. Furthermore, this activity should be abolished following transection of the vagal nerve, and notably, silencing vagal sensory neurons should prevent the creation of sugar preference.

We used fibre photometry[27] to record sugar-evoked responses in the cNST of mice expressing the genetically encoded calcium indicator GCaMP6s in excitatory neurons (*Vglut2-cre*;Ai96; *Vglut2* is also known as *Slc17a6*). To deliver stimuli to the gut, we placed a catheter directly into the duodenal bulb and created an exit port by transecting the intestine about 12 cm distally (Fig. 2a, see Methods). As predicted, our results (Fig. 2b–d) showed robust responses to glucose and MDG. Most notably, all activity was abolished after bilateral transection of the vagal nerves (Fig. 2b–e).

Next, we examined whether cNST neurons activated in response to sugar ingestion indeed receive direct input from vagal ganglion neurons (that is, from the nodose ganglia; see Extended Data Fig. 4a, b). To test this, we used the targeted recombination in active populations (TRAP) system[28,29] to target Cre recombinase to sugar-activated cNST neurons, and used a Cre-dependent monosynaptic retrograde viral reporter to identify their synaptically connected input neurons[30,31].

We infected the cNST with adeno-associated virus (AAV) carrying a Cre-dependent glycoprotein coat and a surface receptor for a transsynaptic reporter virus[30,31], and TRAPed sugar-activated neurons (Fig. 3a; see Extended Data Fig. 4c, d for selectivity of TRAPing). Next, we infected the TRAPed neurons with the retrograde rabies reporter (RABV–dsRed), and investigated whether sugar-activated cNST neurons receive input from vagal ganglion neurons. As controls, we carried out similar experiments but used water or sweetener as TRAPing stimuli. Our results (Fig. 3b, c) revealed large numbers of nodose neurons labelled by the transsynaptic tracing strategy, demonstrating that the sugar-activated cNST neurons receive direct monosynaptic input from the vagal ganglion. By contrast, when we used AceK or water for TRAPing, only a small number of vagal neurons were labelled; we believe these represent activation to licking/drinking or ingestion (Fig. 3b, c).

Finally, we carried out a genetic vagotomy by globally silencing nodose sensory neurons (see Methods), which—as predicted—prevented the development of sugar preference (Extended Data Fig. 3c, d).

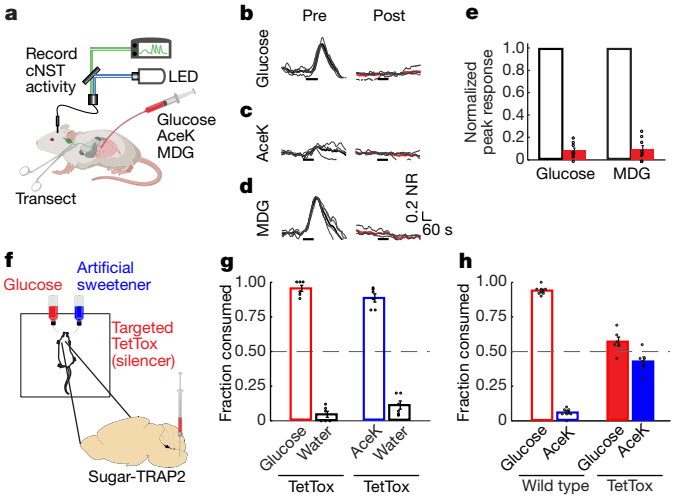

Fig. 2 | Silencing the sugar-activated circuit abolishes sugar preference. a, Fibre photometry monitoring glucose-evoked responses of cNST neurons. The excitatory neurons in the cNST were targeted with GCaMP6s using *VGlut2-cre* mice[46]. **b**–**d**, Neural responses following intestinal delivery of glucose, AceK or MDG. Note strong responses to sugar (**b**) and MDG (**d**). The light traces denote normalized two-trial averages from individual animals and the dark trace is the average of all trials. Black bars below traces indicate the time and duration of stimuli. The average responses after bilateral vagotomy are shown in red (see Methods). Stimuli: 500 mM glucose, 30 mM AceK or 500 mM MDG; $n = 4$ mice. NR, normalized response. **e**, Quantification of neural responses before and after vagotomy. Two-tailed paired *t*-test, $P = 3 \times 10^{-15}$ (glucose), $P = 5 \times 10^{-13}$ (MDG), $n = 4$ mice. Data are mean ± s.e.m. **f**, Schematic of silencing strategy. TRAP2 mice[29] were stimulated with 600 mM glucose to induce expression of Cre recombinase in the cNST. AAV-DIO-TetTox[32] was then targeted bilaterally to the cNST for silencing. **g**, Silencing the sugar-preference neurons in the cNST does not impair the innate attraction to sugar or sweeteners. The graph shows preference for 600 mM glucose versus water, and preference for 30 mM AceK versus water. $n = 6$ mice. Data are mean ± s.e.m. **h**, Sugar-preference graphs (48-h tests) for wild-type mice, demonstrating the robust development of preference for sugar versus sweetener (see also Fig. 1). By contrast, silencing sugar-activated neurons in the cNST abolishes the development of sugar preference. $n = 6$ mice; two-sided Mann–Whitney *U*-test, $P = 4 \times 10^{-4}$; TetTox-silenced animals consumed as much of the AceK sweetener as they did sugar (see also Extended Data Fig. 5). Data are mean ± s.e.m.

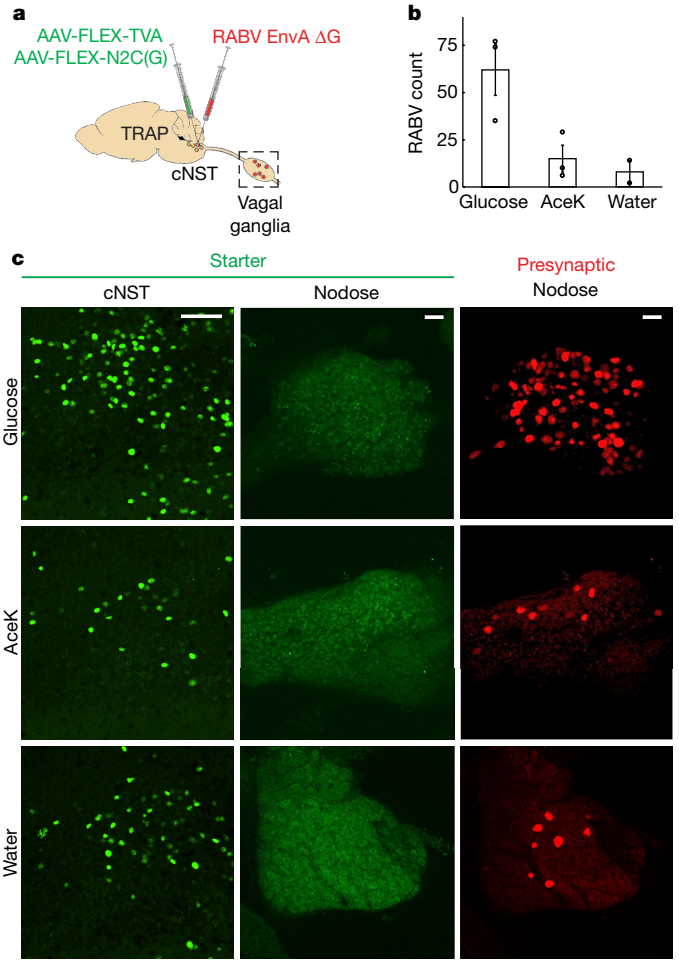

Fig. 3 | Vagal ganglion neurons transmit sugar signals to the brain. a, Strategy for targeting a red fluorescently labelled retrograde transsynaptic rabies reporter (RABV–dsRed)[28,31] to the cNST. Sugar-TRAP neurons in the cNST (designated as 'starter cells')[30,31] were infected with AAVs encoding proteins required for infection with RABV–dsRed, resulting in labelling of the monosynaptic inputs of the sugar-activated cNST neurons by the retrogradely transsynaptic transfer of the RABV–dsRed virus. **b**, Quantification of retrogradely labelled RABV–dsRed neurons in the nodose ganglion. Sugar versus AceK TRAP labelling ($n = 3$ mice). ANOVA, Tukey's HSD post hoc test, $P = 0.0449$. We also performed control TRAP labelling with water ($n = 2$ animals). Sugar versus water TRAP: ANOVA, Tukey's HSD post hoc test, $P = 0.0407$; AceK versus water TRAP: $P = 0.9$. Data are mean ± s.e.m. **c**, Sugar-TRAP cNST neurons (starter, green) receive monosynaptic input from vagal neurons (RABV, red). Note the absence of starter cells in the nodose, confirming that the RABV (red) cells represent retrogradely labelled neurons[30,31]. Scale bars, 100 µm.

Neurons in the cNST mediate sugar preference

If the gut-to-brain sugar-activated cNST neurons are essential for creating preference for sugar, then blocking their function should prevent the formation of sugar preference. Therefore, we engineered mice in which synaptic transmission in the sugar-preference neurons was genetically silenced by targeted expression of tetanus toxin light chain (TetTox)[32]. Our strategy relied on the TRAP system[28,29] to express inducible Cre recombinase in sugar-activated cNST neurons, and bilaterally injecting the cNST with an AAV carrying the Cre-dependent TetTox construct (Fig. 2f, see Methods).

First, we needed to ensure that silencing this circuit did not affect the innate ability of the animals to be attracted to sweet taste, including sugar and sweeteners. Indeed, when the TetTox-targeted mice were tested to choose between sweet or water, they selected the sweet-tasting solutions (either AceK or glucose; Fig. 2g). However, silencing the sugar-activated cNST neurons abolished their capacity to develop a preference for sugar over artificial sweetener, even after prolonged testing sessions (Fig. 2h, Extended Data Fig. 5). These results illustrate the essential role of this circuit in driving the behavioural preference for sugar.

Vagal neurons sensing gut sugar

As information about sugar detection is being transferred via the gut–vagal–brain axis, we set out to directly monitor the activity of this circuit by imaging vagal-neuron responses to gut stimulation with sugar.

We implemented a vagal ganglion functional imaging platform (Fig. 4a) by targeting the genetically encoded calcium indicator GCaMP[33] to vagal sensory neurons[34] (*Vglut2-cre*;Ai96). To visualize the neurons and measure calcium dynamics, we exposed a 1-cm^2 ventral window into the ganglion and used a one-photon microscope equipped with an electron-multiplying CCD camera for imaging[35]. For most imaging sessions, the intestinal segment was exposed to a pre-stimulus application of PBS, then a 10-s (33 µl) or 60-s (200 µl) test stimulus, and a 3-min post-stimulus wash. Neuronal signals were analysed for statistically significant increases in intracellular calcium over baseline (see Methods), and a neuron was classified as a responder if it exhibited responses in more than 60% of the trials[36].

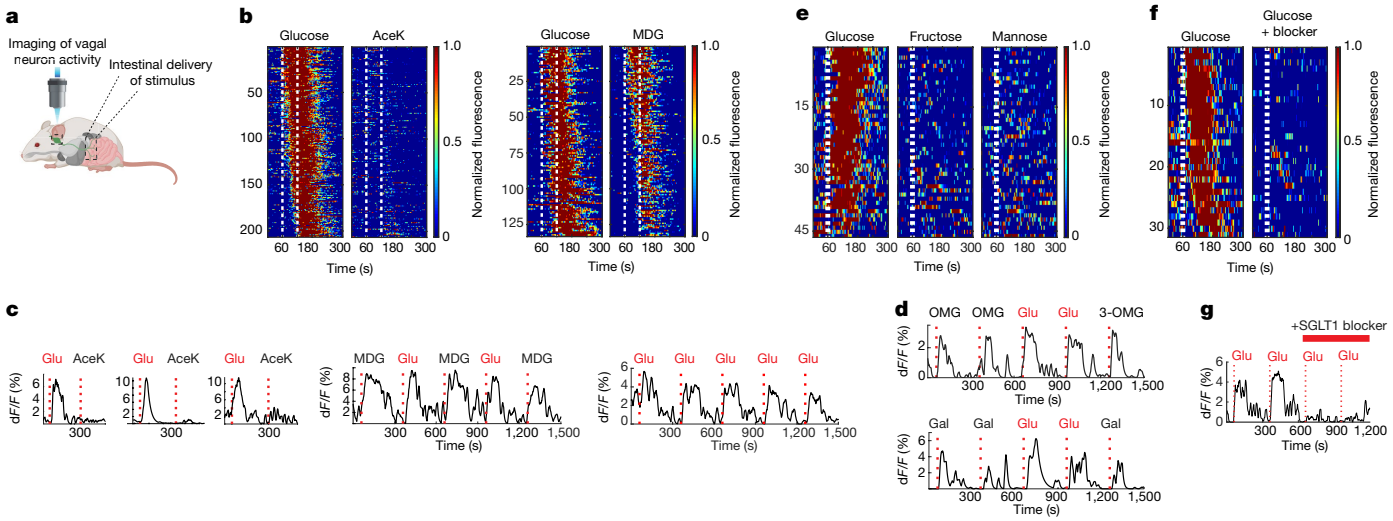

Fig. 4 | Imaging the gut–brain axis. a, We imaged calcium responses in vagal sensory neurons expressing the fluorescent calcium indicator GCaMP6s while stimulating the intestines. **b**, Heat maps depicting *z*-score-normalized fluorescence traces[33,47] from vagal neurons identified as glucose responders. Each row represents the average activity of a single cell to three trials. Stimulus window is shown by dashed white lines. Left, responses of $n = 206$ vagal neurons to a 60-s intestinal infusion of 500 mM glucose; note lack of responses to 30 mM AceK. Right, heat maps depicting $n = 133$ vagal neurons that responded to 60-s infusion of 500 mM glucose, and tested for their responses to 500 mM MDG. Heat maps were normalized across stimuli; responses to glucose and MDG were similar (two-tailed paired *t*-test, $P = 0.06$). **c**, Sample traces of vagal-neuron responses to intestinal stimulation with 60-s pulses of 30 mM AceK and 500 mM glucose from 3 mice (top), or to 10-s pulses of 500 mM glucose and 500 mM MDG (middle and bottom). Note the reliability and rapid onset of responses to the 10-s stimulus (Extended Data Fig. 6c). When using a 10-s stimulus, to minimize potential osmolarity responses (Extended Data Fig. 8), approximately 5% of imaged neurons show statistically significant responses to glucose (Extended Data Fig. 6d). We compared imaging sessions with both the right and left ganglia[25] and did not observe any meaningful difference in the proportion of glucose-responding neurons (Extended Data Fig. 6e). **d**, Vagal-neuron responses to 3-OMG (top) and galactose (bottom), $n = 3$ independent experiments each. These agonists activate vagal neurons in a similar manner to glucose (Extended Data Figs. 2b, 10a, b). **e**, Heat maps of 46 glucose-responding neurons to 500 mM fructose and 500 mM mannose ($n = 5$ ganglia). The monosaccharides fructose and mannose, which are not substrates for SGLT1, do not activate glucose-responsive neurons. Fewer than 10% of glucose responders were activated by either fructose or mannose. **f**, **g**, Summary of responses to a 10-s stimulus of 500 mM glucose for 33 neurons before and after intestinal application 8 mM phlorizin for 5 min ($n = 4$ mice). Responses are severely diminished after blocker application (see Extended Data Fig. 10d, e and Methods).

First, we examined how vagal neurons respond to intestinal delivery of glucose versus sweetener. Delivering glucose into the intestines elicited significant calcium responses in subsets of ganglion neurons (Fig. 4b); we analysed the responses from the vagal ganglia of 8 different mice to a 60-s stimulus of glucose or AceK, and identified around 200 neurons that displayed statistically significant responses to glucose, but less than 1% of these neurons displayed stimulus-dependent activity to AceK (Fig. 4b). As expected, intestinal delivery of MDG also activated the majority of vagal neurons that responded to glucose (Fig. 4b, c, Extended Data Fig. 6a).

Next, we assessed the reliability and temporal causality of the vagal responses by reducing the stimulus window from 60 s to 10 s. Our results showed that vagal responses to intestinal glucose are robust and reliable[37] (Fig. 4c, Extended Data Fig. 6b, c). Overall, we examined 51 ganglia and 4–5% of GCaMP-expressing neurons (205 out of 4,803 neurons) responded to the 10-s glucose stimulus (Extended Data Fig. 6d).

As neurons in the nodose ganglion innervate the gut[21] (that is, the source of the gut–brain signal), the cell bodies of the sugar-sensing neurons in the nodose ganglion should be retrogradely labelled by applying a tracer from their afferents in the gut[26]. Thus, we injected fluorescently conjugated cholera toxin subunit B (CTB)[38] into the duodenum of GCaMP-expressing mice (Extended Data Fig. 7a), and examined the labelled duodenal innervating neurons for responses to intestinal delivery of sugar. Indeed, around 20% of the duodenum back-filled vagal sensory neurons robustly responded to glucose (Extended Data Fig. 7b, c).

We note that a previous study reported the characterization of candidate nutrient-sensing neurons in the nodose ganglia[24]. These neurons responded indiscriminately to high concentrations of several stimuli, including 1 M glucose and 0.5 M salt. Our results show that such responses, which are largely independent of the quality of the stimulus, are not glucose-sensing nor are they required for the development of sugar preference, but rather represent responses to a wide range of high-osmolarity stimuli (Extended Data Figs. 8, 9).

SGLT1 transduces gut–brain sugar signals

We reasoned that the gut-to-brain signal might depend on known sugar sensors recruited into this role, perhaps in a dedicated subpopulation of gut cells. Although the sweet-taste receptor is expressed in enteroendocrine cells[39], it is not involved in this process, as sweet-taste receptor knockout (T1R2/3 KO) mice still exhibited normal sugar-preference behaviour (Fig. 1c).

The principal glucose transporter (and sensor) in the intestine is the sodium–glucose-linked transporter-1 (SGLT1)[19,40]. This transporter is expressed in enterocytes as well as in enteroendocrine cells that secrete a wide range of hormones and bioactive molecules and are thought to also function as a conduit between the gut and the vagal nerve[41,42]. Therefore, we investigated whether SGLT1 is required to transmit the gut-to-brain sugar signal by determining whether other substrates of SGLT1—galactose and the glucose analogue 3-*O*-methyl-D-glucose (3-OMG)[19]—also activate the same vagal neurons as glucose. Indeed, neurons responding to intestinal glucose were also stimulated by 3-OMG and galactose (Fig. 4d, Extended Data Fig. 10a, b). Critically, this circuit is dedicated to glucose, as other caloric sugars such as fructose and mannose (that are not substrates of SGLT1)[19] do not activate the glucose-responsive vagal neurons (Fig. 4e, Extended Data Fig. 10c), do not create a behavioural preference (Extended Data Fig. 8e), but still trigger osmolarity responses (Extended Data Fig. 8).

Next, we assessed whether pharmacological inhibition of SGLT1 abolishes the glucose-dependent neuronal responses. We examined the responses to two consecutive 10-s stimuli of intestinal glucose before and after a 5-min wash of the intestinal segment with phlorizin[19], an SGLT1 blocker. Our results (Fig. 4f, g, Extended Data Fig. 10d, e), demonstrated a marked loss of glucose responses following intestinal application of phlorizin[19]. Together, these results place SGLT1 as an important component of the sugar-preference signalling circuit. It will be of interest to determine the identity of the intestinal cells mediating these responses, as they represent another potential target for modulating this circuit.

Co-opting the sugar-preference circuit

The results presented above reveal a specific circuit via the vagal ganglia to the brain critical for driving the development of preference for sugar. We devised an experiment to determine whether the selective activation of this circuit can be recruited to create a preference to a previously less-preferred stimulus. Our strategy was to identify a genetic driver that marks sugar-preference neurons in the cNST, and then link their activation to the ingestion of a novel stimulus.

We examined the Allen Brain Atlas for candidate genes with enriched expression in the cNST, and tested candidates for glucose-evoked Fos labelling (Fig. 5a). Our results demonstrated that proenkephalin (*Penk*)-expressing neurons in the cNST[43], marked by a *Penk-cre* construct driving tdTomato (*Penk-cre*;Ai75D), respond strongly to sugar stimuli (Fig. 5b, c); approximately 85% of the sugar-induced Fos-labelled neurons in the cNST are *Penk*-positive, and over 80% of the *Penk*-positive neurons were labelled by Fos after sugar ingestion.

We injected a Cre-dependent AAV encoding the excitatory designer receptor hM3Dq[44] into the cNST of *Penk-cre* mice, so that *Penk* cNST neurons could be experimentally activated by the hM3Dq agonists clozapine *N*-oxide or clozapine[44,45]. After 8 days to allow for receptor expression, mice were exposed to two-bottle preference assays using artificially sweetened cherry-flavoured versus grape-flavoured solutions (Fig. 5d). Under this paradigm, the cherry solution was made sweeter than grape (see Methods) so that the animals would be significantly more attracted to the cherry flavour (Fig. 5e). Next, we introduced clozapine into the less-preferred grape flavour, and investigated whether clozapine-mediated activation of the *Penk* cNST neurons (much like glucose-mediated activation) can create a new preference. Indeed, after 48 h of exposure to the grape plus clozapine bottle, mice completely switched their preference, even though the grape solution was far less sweet than the cherry solution (Fig. 5e, purple lines). To demonstrate that the preference switch is independent of the nature of the initially less-preferred stimuli, we flipped the starting flavours so that cherry was less favoured, and obtained an equivalent switch in preference (Fig. 5e, red lines). As anticipated, wild-type mice without the designer receptor were indifferent to clozapine and continued to prefer the sweeter solution (Fig. 5f). These results demonstrate that artificial activation of the sugar-preference circuit is sufficient to drive the development of a novel preference to an otherwise low-preference stimulus.

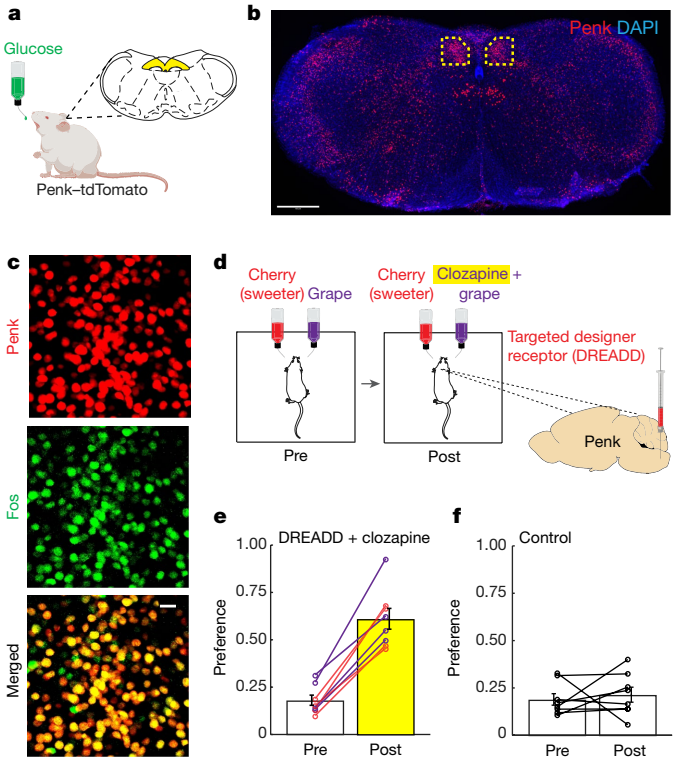

Fig. 5 | Activation of sugar-responsive cNST neurons confers novel flavour preference. a–**c**, *Penk-cre* mice were stimulated with 600 mM glucose and brain slices were analysed for Fos and *Penk* labelling. *Penk* neurons were marked by expression of nuclear-localized tdTomato (Ai75D reporter line)[48]. **b**, Low-magnification section of the brain stem (bregma − 7.5 mm) showing *Penk* expression (red); tissue was counterstained with DAPI (blue). $n = 2$ independent experiments. Scale bar, 500 µm; cNST, yellow box. **c**, Sugar-preference neurons express *Penk*. *Penk* neurons labelled with tdTomato (from **b**) and glucose-activated neurons (Fos-labelled) marked green. Note the high degree of overlap in the merged image. Approximately 85% of sugar-activated cNST neurons are marked by *Penk*, and about 90% of cNST *Penk* neurons show sugar-Fos labelling ($n = 3$ mice). Scale bar, 20 µm. **d**, Expression of activating DREADD receptor[44,45] (via AAV-DIO-hM3Dq) was targeted bilaterally to the cNST of *Penk-cre* mice. The mice were then tested for their preference between two flavours for 48 h (Pre). Shown is an example using cherry (containing 2 mM AceK) versus grape (with 1 mM AceK). Mice were conditioned and tested using the less-preferred flavour plus the DREADD agonist clozapine (Post; see Methods). **e**, *Penk*-hM3Dq mice initially prefer the sweeter solution. After associating clozapine-mediated activation of *Penk* cNST neurons with the less-preferred flavour, all the *Penk*-hM3Dq mice switched their preference (Pre, 18.1 ± 2.7%; Post, 61.1 ± 5.5%; $n = 8$ mice; two-sided Mann–Whitney *U*-test, $P = 1 \times 10^{-4}$). The experiment was carried out using grape (purple lines) or cherry (red lines) as the initially less-preferred stimuli. **f**, Mice not expressing the DREADD receptor are unaffected by the presence of clozapine (Pre, 19.0 ± 3.0%; Post, 21.4 ± 4.0%; $n = 8$ mice); control mice were subjected to the same conditioning and testing as the experimental cohort. Values are mean ± s.e.m.

Discussion

Sugar is an essential energy source across all animal species, and it is therefore expected that selective circuits be dedicated to seek, recognize and motivate its consumption. The discovery of this gut-to-brain circuit provides a powerful pathway to help to meet these needs.

In this study, we show that glucose acts in the gut to activate a neural circuit that communicates to the brain the presence of sugar. What is the advantage of a gut-to-brain sugar-detection system in addition to the taste system? A post-ingestive sensing system in the gut assures that signalling only occurs after the sugar molecules reach their desired target for effective absorption and metabolic consumption. The association between the activation of this gut-to-brain circuit paired with the recognition of sugar by the taste system affords animals the fundamental capacity to identify, develop and reinforce a strong and durable preference for sugar-rich food sources. The evolutionary association of these two separate circuits combines nutrition with the basic sense of taste. In the future, it would be of interest to determine whether preference for other essential nutrients also utilizes this gut–brain axis.

Notably, artificial sweeteners were introduced in consumer products more than four decades ago; however, their overall impact in decreasing sugar consumption, preference and craving has been negligible. This may now be understood at the circuit level (that is, as—in contrast

to sugar—they do not activate the preference circuit), and implies that it may be possible to develop a new class of sweeteners that activate both the sweet-taste receptor in the tongue and the gut–brain axis, and consequently help to moderate the strong drive to consume sugar.

Online content

Any methods, additional references, Nature Research reporting summaries, source data, extended data, supplementary information, acknowledgements, peer review information; details of author contributions and competing interests; and statements of data and code availability are available at https://doi.org/10.1038/s41586-020-2199-7.

1. Sclafani, A., Marambaud, P. & Ackroff, K. Sucrose-conditioned flavor preferences in sweet ageusic T1r3 and Calhm1 knockout mice. *Physiol. Behav.* **126**, 25–29 (2014).
2. de Araujo, I. E. et al. Food reward in the absence of taste receptor signaling. *Neuron* **57**, 930–941 (2008).
3. Yarmolinsky, D. A., Zuker, C. S. & Ryba, N. J. P. Common sense about taste: from mammals to insects. *Cell* **139**, 234–244 (2009).
4. Zuker, C. S. Food for the brain. *Cell* **161**, 9–11 (2015).
5. Elliott, Perry. & Elliott, P. *Production of Sugar in the United States and Foreign Countries* (US Department of Agriculture, 1917).
6. *Sugar and Sweeteners Yearbook Tables* https://www.ers.usda.gov/data-products/sugar-and-sweeteners-yearbook-tables/#U.S.%20Consumption%20of%20Caloric%20Sweeteners (US Department of Agriculture, 2019).
7. Nelson, G. et al. Mammalian sweet taste receptors. *Cell* **106**, 381–390 (2001).
8. Spector, A. C. & Travers, S. P. The representation of taste quality in the mammalian nervous system. *Behav. Cogn. Neurosci. Rev.* **4**, 143–191 (2005).
9. Wang, L. et al. The coding of valence and identity in the mammalian taste system. *Nature* **558**, 127–131 (2018).
10. Scott, K. Taste recognition: food for thought. *Neuron* **48**, 455–464 (2005).
11. Peng, Y. et al. Sweet and bitter taste in the brain of awake behaving animals. *Nature* **527**, 512–515 (2015).
12. Wang, Z., Singhvi, A., Kong, P. & Scott, K. Taste representations in the *Drosophila* brain. *Cell* **117**, 981–991 (2004).
13. Sclafani, A., Zukerman, S. & Ackroff, K. Postoral glucose sensing, not caloric content, determines sugar reward in C57BL/6J mice. *Chem. Senses* **40**, 245–258 (2015).
14. Ren, X. et al. Nutrient selection in the absence of taste receptor signaling. *J. Neurosci.* **30**, 8012–8023 (2010).
15. Zhang, Y. et al. Coding of sweet, bitter, and umami tastes: different receptor cells sharing similar signaling pathways. *Cell* **112**, 293–301 (2003).
16. Pérez, C. A. et al. A transient receptor potential channel expressed in taste receptor cells. *Nat. Neurosci.* **5**, 1169–1176 (2002).
17. Sclafani, A. Gut–brain nutrient signaling. Appetition vs. satiation. *Appetite* **71**, 454–458 (2013).
18. Zukerman, S., Ackroff, K. & Sclafani, A. Post-oral appetite stimulation by sugars and nonmetabolizable sugar analogs. *Am. J. Physiol. Regul. Integr. Comp. Physiol.* **305**, R840–R853 (2013).
19. Wright, E. M., Loo, D. D. F. & Hirayama, B. A. Biology of human sodium glucose transporters. *Physiol. Rev.* **91**, 733–794 (2011).
20. Sheng, M. & Greenberg, M. E. The regulation and function of c-fos and other immediate early genes in the nervous system. *Neuron* **4**, 477–485 (1990).
21. Berthoud, H.-R. & Neuhuber, W. L. Functional and chemical anatomy of the afferent vagal system. *Auton. Neurosci.* **85**, 1–17 (2000).
22. Sclafani, A. & Glendinning, J. I. Flavor preferences conditioned in C57BL/6 mice by intragastric carbohydrate self-infusion. *Physiol. Behav.* **79**, 783–788 (2003).
23. Zukerman, S., Ackroff, K. & Sclafani, A. Rapid post-oral stimulation of intake and flavor conditioning by glucose and fat in the mouse. *Am. J. Physiol. Regul. Integr. Comp. Physiol.* **301**, R1635–R1647 (2011).
24. Williams, E. K. et al. Sensory neurons that detect stretch and nutrients in the digestive system. *Cell* **166**, 209–221 (2016).
25. Han, W. et al. A neural circuit for gut-induced reward. *Cell* **175**, 665–678.e23 (2018).
26. Kaelberer, M. M. et al. A gut–brain neural circuit for nutrient sensory transduction. *Science* **361**, eaat5236 (2018).
27. Gunaydin, L. A. et al. Natural neural projection dynamics underlying social behavior. *Cell* **157**, 1535–1551 (2014).
28. Guenthner, C. J., Miyamichi, K., Yang, H. H., Heller, H. C. & Luo, L. Permanent genetic access to transiently active neurons via TRAP: targeted recombination in active populations. *Neuron* **78**, 773–784 (2013).
29. Allen, W. E. et al. Thirst-associated preoptic neurons encode an aversive motivational drive. *Science* **357**, 1149–1155 (2017).
30. Callaway, E. M. & Luo, L. Monosynaptic circuit tracing with glycoprotein-deleted rabies viruses. *J. Neurosci.* **35**, 8979–8985 (2015).
31. Reardon, T. R. et al. Rabies virus CVS-N2c$^{\Delta G}$ strain enhances retrograde synaptic transfer and neuronal viability. *Neuron* **89**, 711–724 (2016).
32. Yamamoto, M. et al. Reversible suppression of glutamatergic neurotransmission of cerebellar granule cells in vivo by genetically manipulated expression of tetanus neurotoxin light chain. *J. Neurosci.* **23**, 6759–6767 (2003).
33. Chen, T. W. et al. Ultrasensitive fluorescent proteins for imaging neuronal activity. *Nature* **499**, 295–300 (2013).
34. Chang, R. B., Strochlic, D. E., Williams, E. K., Umans, B. D. & Liberles, S. D. Vagal sensory neuron subtypes that differentially control breathing. *Cell* **161**, 622–633 (2015).
35. Lee, H., Macpherson, L. J., Parada, C. A., Zuker, C. S. & Ryba, N. J. P. Rewiring the taste system. *Nature* **548**, 330–333 (2017).
36. Barretto, R. P. J. et al. The neural representation of taste quality at the periphery. *Nature* **517**, 373–376 (2015).
37. Mei, N. Vagal glucoreceptors in the small intestine of the cat. *J. Physiol.* **282**, 485–506 (1978).
38. Conte, W. L., Kamishina, H. & Reep, R. L. The efficacy of the fluorescent conjugates of cholera toxin subunit B for multiple retrograde tract tracing in the central nervous system. *Brain Struct. Funct.* **213**, 367–373 (2009).
39. Dyer, J., Salmon, K. S. H., Zibrik, L. & Shirazi-Beechey, S. P. Expression of sweet taste receptors of the T1R family in the intestinal tract and enteroendocrine cells. *Biochem. Soc. Trans.* **33**, 302–305 (2005).
40. Geillinger, K. E. et al. The role of SGLT1 and GLUT2 in intestinal glucose transport and sensing. *PLoS ONE* **9**, e89977 (2014).
41. Latorre, R., Sternini, C., De Giorgio, R. & Greenwood-Van Meerveld, B. Enteroendocrine cells: a review of their role in brain–gut communication. *Neurogastroenterol. Motil.* **28**, 620–630 (2016).
42. Chambers, A. P., Sandoval, D. A. & Seeley, R. J. Integration of satiety signals by the central nervous system. *Curr. Biol.* **23**, R379–R388 (2013).
43. Lein, E. S. et al. Genome-wide atlas of gene expression in the adult mouse brain. *Nature* **445**, 168–176 (2007).
44. Armbruster, B. N., Li, X., Pausch, M. H., Herlitze, S. & Roth, B. L. Evolving the lock to fit the key to create a family of G protein-coupled receptors potently activated by an inert ligand. *Proc. Natl Acad. Sci. USA* **104**, 5163–5168 (2007).
45. Gomez, J. L. et al. Chemogenetics revealed: DREADD occupancy and activation via converted clozapine. *Science* **357**, 503–507 (2017).
46. Vong, L. et al. Leptin action on GABAergic neurons prevents obesity and reduces inhibitory tone to POMC neurons. *Neuron* **71**, 142–154 (2011).
47. Peron, S., Chen, T.-W. & Svoboda, K. Comprehensive imaging of cortical networks. *Curr. Opin. Neurobiol.* **32**, 115–123 (2015).
48. Daigle, T. L. et al. A suite of transgenic driver and reporter mouse lines with enhanced brain-cell-type targeting and functionality. *Cell* **174**, 465–480.e22 (2018).

Methods

Mice

All procedures were carried out in accordance with the US National Institutes of Health (NIH) guidelines for the care and use of laboratory animals, and were approved by the Institutional Animal Care and Use Committee at Columbia University. Adult animals older than 6 weeks of age and from both genders were used in all experiments. C57BL/6J (JAX 000664), *Arc-creER* (TRAP, JAX 021881), TRAP2 (JAX 030323), *TRPM5* KO (JAX 013068), T1R2/3 KO (generated in house, JAX 013065 and 013066), Ai96 (JAX 028866), *VGlut2*-IRES-Cre (JAX 028863), *Gpr65*-IRES-Cre (JAX 029282), *Penk*-IRES2-Cre (JAX 025112), Ai75D (JAX 025106) and R26-TeNT (MGI 3839913).

Fos stimulation and immunohistochemistry

Animals were water restricted for 23 h, given access to 1 ml of water for 1 h, and then water restricted again for another 23 h. The stimulus consisted of 600 mM glucose, 600 mM MDG, 600 mM sucrose, 600 mM 3-OMG, 600 mM galactose, 30 mM AceK or milliQ water for a period of 90 min in the absence of food. For intra-gastric infusion experiments, food was removed from the cage 12 h before stimulus infusion. A syringe pump microcontroller (Harvard Apparatus) was used to deliver 1.5 ml of the stimulus solution at 0.075 ml min^{-1}. After 90 min, mice were perfused transcardially with PBS followed by 4% paraformaldehyde. Brains were dissected, and fixed overnight in paraformaldehyde at 4 °C. The brains were sectioned coronally at 100 µm, and labelled with anti-c-Fos (Santa Cruz, sc-52 goat, 1:500; or SYSY, no. 226004 guinea pig, 1:5,000) in 5% normal donkey serum (EMD Millipore, Jackson ImmunoResearch) in 0.3% Triton X-100 in 1× PBS for 48 h at 4 °C with gentle shaking, and then Alexa Fluor 488-, 568- or 647-conjugated donkey anti-goat or anti-guinea pig (Jackson ImmunoResearch) in 5% normal donkey serum in 0.3% Triton X-100 in 1× PBS for 24 h at 4 °C with gentle shaking. Images were acquired using an Olympus FluoView 1000 confocal microscope. Larger field-of-view images were acquired using a Nikon AZ100 Multizoom Slide Scanner. Quantification of Fos-labelled neurons was done by manual counting in a 300 × 300 µm region of interest (ROI) in the right cNST.

For intragastric stimulation, animals were anaesthetized with ketamine and xylazine (100 mg kg^{-1} and 10 mg kg^{-1}, intraperitoneal). The stomach was exteriorized through an abdominal incision, and a Silastic (Dow Corning) tubing was inserted into the forestomach region and secured with silk sutures[49]. The other end was tunnelled subcutaneously along the left flank and exteriorized at the dorsal neck area. Mice were individually housed and allowed to recover for at least 5 days before stimulus infusion.

Two-bottle preference assays

The preference-switch experiments were carried out in standard mouse cages holding a custom designed 3D-printed scaffold for two bottles. Each bottle was outfitted with an electronic licking sensor, and access to the licking spout was controlled by a mechanical shutter. Mice were not water deprived before the experiment and had ad libitum access to food throughout. For behavioural tests, mice were first tested for their initial preference by completing 100 drinking trials. Each trial consisted of a choice between 600 mM glucose (or 600 mM MDG) and 30 mM AceK. Trials lasted 5 s and were initiated after the first lick to either bottle; inter-trial intervals were 40 s. To familiarize animals with the two choices, mice were required to complete 500 licks to 600 mM glucose alone, and 30 mM AceK alone; this was repeated twice. Animals were tested for their sugar (or MDG) versus sweetener preference over 36 h using 5-s trials. Preference indexes: Pre, the number of licks to glucose divided by the total number of licks during the first 100 trials of baseline measurements; Post, the number of licks to glucose divided by the total number of licks during the last 100 trials of the behavioural session. Because T1R2/3 double knockouts cannot taste sweet, they are often averse to the 'bitter' in high concentrations of AceK (that is, not being countered by its high sweetness), therefore they were tested with 300 mM sucrose versus 5 mM AceK.

Molecular cloning of custom pAAV constructs

pAAV.hSyn.FLEX-eGFP-Rpl10a.WPRE.hGH-pA is constructed by ligation of two fragments: the eGFP pAAV backbone fragment was generated by digestion of pAAV-FLEX-EGFPL10a, a gift from N. Heintz, A. Nectow and E. Schmidt (Addgene plasmid 98747), with MluI and KpnI, and the hSyn fragment with corresponding restriction ends was generated from pAAV-hSyn-DIO-hM4D(Gi)-mCherry, a gift from B. Roth (Addgene plasmid 44362).

pAAV.CBA.FLEX-GFP-TeTx.WPRE.bGH-pA (TetTox) DNA is a gift from P. Wolff[50].

All pAAVs were amplified in *recA1*$^-$ NEB Stable cells and extracted by maxiprep (Zymo Research), and serotype 2/9 AAVs were produced by the Janelia Farms viral core.

Genetic access to sugar-preference neurons

The TRAP[28,29,51] strategy was used in TRAP2 mice to gain genetic access to sugar-activated neurons in the cNST. The 4-hydroxytamoxifen (4OHT, Sigma H6278) was prepared as previously described[51]. AAV-injected TRAP2 mice were singly housed, water restricted for 23 h, given access to 1 ml of water for 1 h, water restricted again for another 23 h, and then presented with 600 mM glucose (or 30 mM AceK) ad libitum, in the absence of food and nesting material. After 1 h, mice were injected intraperitonially with 12.5 mg kg^{-1} 4OHT, and placed back to the same cage for an additional 3 h. At the end of the 4 h of sugar or AceK exposure, mice were returned to regular home-cage conditions (group-caged, with nesting material, ad libitum food and water). Mice were used for experiments a minimum of 7 days after this TRAP protocol.

Stereotaxic surgery

For stereotaxic injections of reporter virus, mice were anaesthetized with ketamine and xylazine (100 mg kg^{-1} and 10 mg kg^{-1}, intraperitoneal), and placed into a stereotaxic frame with a closed-loop heating system to maintain body temperature. For retrograde monosynaptic tracing, animals were unilaterally injected with 100 nl of a 1:1 mixture of AAVs carrying Cre-dependent rabies TVA and glycoprotein G (AAV1 EF1a-FLEX-TVA-mCherry, UNC vector core, and AAV1 FLEX-nGFP-2A-N2c(G) (a gift from T. Reardon)[31], and a pseudotyped rabies virus carrying dsRed (RABV N2C(Delta G)-dsRed-EnvA, a gift from T. Reardon)[31]. cNST coordinates (Paxinos stereotaxic coordinates[52]) used for injections are relative to bregma and skull surface: caudal 7.5 mm, lateral ±0.3 mm, ventral 3.7–4 mm.

Monosynaptic retrograde tracing and silencing experiments

For retrograde monosynaptic tracing, Arc-CreER (TRAP)[28] mice were allowed to recover 3 weeks after AAV injection, and the TRAP procedure was carried out as described above, except that 4OHT was prepared in corn oil[28], and was injected 1 h before stimulus presentation. After 7 days, EnvA-RABV was injected into the same site. Mice were euthanized 2 weeks after the RABV injection and examined for expression of starter cells (nGFP and dsRed) and their monosynaptic inputs (dsRed)[30,31].

For synaptic inhibition experiments, sugar-TRAP cNST neurons were bilaterally injected with 300 nl of AAV carrying Cre-dependent TetTox (AAV9 CBA.FLEX-TetTox)[50].

Synaptic-silencing experiments

C57BL/6J and Trap2[29,51] mice expressing TetTox in the cNST were tested in the two-bottle sugar versus sweetener preference assay for 48 h. For the first day, mice were acclimatized by exposure to AceK versus water, the second they were given glucose versus water, and the third and fourth days they were tested for their preference to sugar versus sweetener. To ensure silencing did not affect sweet-taste detection,

mice were also examined for their attraction to sugar versus water (second day) as well as artificial sweetener versus water (first day). Fraction consumed for sugar versus AceK on days 3–4 were calculated as (volume of glucose consumed)/(total volume consumed). Fraction consumed for AceK versus water was calculated as (volume of AceK consumed)/(total volume consumed).

Fibre photometry, gut stimulus delivery and vagotomy

Vglut2-cre;Ai96 animals were placed in a stereotaxic frame and implanted with a 400 µm core, 0.48 NA optical fibre (Doric Lenses) 50–100 µm over the right cNST. Photometry experiments were conducted a minimum of 13 days after fibre implantation surgery. Real-time population-level GCaMP fluorescence was recorded using a RZ5P fibre photometry system with Synapse software (Tucker Davis Technologies) as described previously[53]. In brief, sinusoidally modulated 465 nm and 405 nm light from light-emitting diodes (Doric Lenses) were combined via a multi-port fluorescence mini-cube into a fibre patch-cord connected to the mouse, and real-time demodulated emission signals were saved offline for analysis. Calcium-dependent signals $F_{465\,nm}$ were compared with calcium-independent GCaMP fluorescence $F_{405\,nm}$ to control for movement and bleaching artefacts. The data was de-trended by first applying a least-squares linear fit to produce $F_{fitted\,405\,nm}$, and dF/F was calculated as $(F_{465\,nm} - F_{fitted\,405\,nm})/F_{fitted\,405\,nm}$ (ref. [27]). Data from each mouse were then normalized to peak fluorescence (calculated as a 10-s window around the peak point), and presented as normalized responses. For each stimulus, the normalized two-trial average was plotted and smoothed over a moving average. To quantify effects of vagotomy, we calculated the ratio of stimulus-related peak amplitude of the normalized trace (within 120 s of stimulus onset) before and after the procedure.

To deliver intestinal stimuli, all animals were anaesthetized with ketamine and xylazine (100 mg kg^{-1} and 10 mg kg^{-1}, intraperitoneal), re-dosing was performed as necessary with ketamine only (33 mg kg^{-1}). Mice were immobilized as previously described[36], positioned in a supine position, with the head rigidly secured using the metal bar. To ensure a clear airway, the mouse was tracheotomized. An incision was made into the greater curvature of the stomach, the tip of the catheter was inserted past the pyloric sphincter and secured by a suture into the duodenal bulb. Another suture was tied around the catheter and stomach to prevent spillage of gastric contents. Upon implantation of the catheter, the intestines were filled with 1 ml of PBS and an exit port cut at the most distally inflated intestinal segment, approximately 12 cm from the catheter. The intestines were flushed with PBS for 5 min at 150 µl min^{-1} before the beginning of each experiment. Stimulus delivery was performed via a series of peristaltic pumps (BioChem Fluidics) operated via custom Matlab software/ Arduino microcontroller. Stimuli and washes were delivered through separate lines that converged on a common perfusion manifold (Warner Instruments) connected to the duodenal catheter. All trials were 7-min long and consisted of a 120-s baseline (PBS 150 µl min^{-1}), a 60-s stimulus (200 µl min^{-1}), and a 4-min washout period (180 s at 600 µl min^{-1}, and 60 s at 150 µl min^{-1}). Stimuli were each presented twice in an interleaved fashion. All chemicals were obtained from Sigma and dissolved in 1× PBS at the following concentrations: 30 mM AceK, 500 mM glucose and 500 mM MDG.

The vagotomy procedure was carried out immediately after the first round of stimuli. Salivary glands were cauterized and removed. Then, skin around the tracheotomy tube was retracted to expose the cervical trunk of the vagus nerve running in close proximity to the carotid artery. The nerve was carefully dissected from the underlying vessels using fine Dumont forceps and fully transected by a pair of Vannas scissors[54].

Genetic vagal silencing experiments

Vglut2-cre animals were anaesthetized with ketamine and xylazine (100 mg kg^{-1} and 10 mg kg^{-1}, intraperitoneal). Ophthalmic ointment was applied to the eyes, and subcutaneous injections of carprofen (5 mg kg^{-1}) and buprenorphine (0.05 mg kg^{-1}) were given to each mouse before surgery. The skin under neck was shaved and betadine and alcohol were used to scrub the skin three times. A midline incision (~1.5 cm) was made and the trachea and surrounding muscles were gently retracted to expose the nodose ganglia. Then, AAV9 CBA.FLEX-TetTox (600 nl per ganglion) containing Fast Green (Sigma, F7252-5G) was injected in both left and right ganglia using a 30° bevelled glass pipette and Nanolitre 2000 microinjector positioned with a micromanipulator. Virus was injected in 60-nl pulses and ganglion targeting was visualized with the dye. At the end of surgery, the skin incision was closed using 5-0 absorbable sutures (CP medical, 421A). Mice were allowed to recover for a minimum of 26 days before behavioural testing. We note that 50% of the animals survived the surgical procedure and bilateral injections.

Vagal calcium imaging

Vglut2-cre;Ai96 or Gpr65-Cre;Ai96 mice were anaesthetized, tracheotomized, and positioned on a surgical platform (Thorlabs breadboard). The nodose ganglion was then exposed by severing the posterior tendon of the digastric muscle, cauterizing the occipital branch of the carotid artery and dissecting the trunk of the nerve. Then the preparation was affixed to a set of manual goniometric stages (Newport Instruments) allowing for angular rotation about the longitudinal and lateral axes for optimal positioning under the microscope. Imaging was as previously described[35]. Imaging data was obtained using an Evolve 512 EMCCD camera (Photometrics). Data was acquired at 10 Hz. A single field of view was chosen for recording and analysis from each mouse, each containing 80–150 segmented single neurons.

To deliver intestinal stimuli for nodose calcium imaging, the duodenum was also exposed and catheterized as described above. A typical trial was 5 min long and consisted of a 60-s baseline (PBS 150 µl min^{-1}), a 10-s (or 60-s) stimulus (200 µl min^{-1}), and a 3-min washout period (120 s at 600 µl min^{-1}, 30 s at 1,800 µl min^{-1}, and 30 s at 150 µl min^{-1}). Chemicals were dissolved in PBS: AceK, 30mM; glucose, 500 mM, MDG, 500 mM; mannitol, 500 mM; galactose, 500 mM; 3-OMG, 500 mM. For SGLT1 blocker experiments, 8 mM phlorizin (Sigma) was dissolved in PBS with 3% w/v 1 M NaOH (0.03 M NaOH final)[18], which was titrated back to pH 7.4. The blocker was used within 30 min of preparation. The intestines were pre-washed with PBS + phlorizin flowing at 150 µl min^{-1} for 5 min before commencing the experiments, glucose 500 mM was diluted in PBS + 8 mM phlorizin.

For retrograde labelling of vagal neurons from the duodenum, recombinant Alexa Fluor 594-conjugated CTB (Invitrogen C34777) was injected into the wall of the intestines. A total of 3 µl of 10 mg ml^{-1} (1%) CTB was injected across 10 sites in the duodenum (within 2 cm of the pylorus) using a 30° bevelled glass pipette connected to a Nanolitre 2010 microinjector (WPI). The pipette was inserted into the outer muscular layer of the intestines (that is, not luminally) at an acute angle. Mice were used for calcium imaging experiments 3–5 days after CTB injection.

Calcium-imaging data collection and analysis

Calcium-imaging data collected at 10 Hz was downsampled by a factor of 3, and the images stabilized using the NoRMCorre algorithm[55]. Motion corrected movies were then manually segmented in ImageJ using the Cell Magic Wand plugin (https://www.maxplanckflorida.org/fitzpatricklab/software/cellMagicWand/). Only ROIs whose average fluorescence was greater than the surrounding neuropil in more than 10% of frames were used for further analysis. Neuropil fluorescence was subtracted from each ROI with the FISSA toolbox[56], and neural activity was denoised using the OASIS deconvolution algorithm[57].

Neuronal activity was analysed for significant stimulus-evoked responses, as described in ref. [36], with the following modifications. To determine the baseline to calculate *z*-scores, traces were smoothed over a 15-s moving window, and a baseline distribution of deviations from the median for each cell over the entire experiment was calculated using

periods preceding the stimulus onset. This baseline was then used to calculate a modified *z*-score by subtracting the median and dividing by the median absolute deviation. Trials with an average modified *z*-score above 1.6 for the 90 s following presentation of the stimulus were classified as responding trials, and a cell was required to respond in more than 60% of stimulus trials to be classified as a responder. This criterion was validated against visual identification of responses by independent investigators and accurately identified >90% of the same cells with less than 5% false-positive rate. Only cells that reached at least 2% d*F*/*F* for the first two trials of glucose were included in heat maps. Heat maps for each experiment were normalized across stimuli, so different stimuli are directly comparable. We note that there were no significant numbers of MDG-only responses (~95% of the neurons that responded to MDG also responded to glucose; a total of 168 MDG responders were analysed and 159 showed responses to both). For the blocker and control data (Fig. 4, Extended Data Fig. 10) responses were filtered to ensure reliable trials preceding blocker addition (that is, the two responses before blocker addition had to be within 70% of each other).

Chemogenetic-activation experiments

For gain of preference experiments, *Penk-cre* animals were stereotaxically injected with 300 nl of AAV carrying Cre-dependent activator DREADD ($1–2 \times 10^{13}$ GC ml^{-1}; AAV9 Syn-DIO-hM3Dq-mCherry, Addgene 44361), bilaterally in the cNST. At least 8 days was allowed for recovery and viral expression before behavioural testing. We note that in control studies, we validated that injections into the cNST did not infect vagal neurons. We examined six different ganglia with thousands of neurons and detected a total of only four labelled neurons (see also Fig. 3c for an example with AAV1).

C57BL/6J and *Penk* mice expressing hM3Dq in the cNST were tested in a two-bottle grape versus cherry flavour-preference assay. Grape solution was 0.39 g l^{-1} Kool-Aid Unsweetened Grape (00043000955635) in 1 mM AceK in milliQ water; cherry solution was 0.9 g l^{-1} Kool-Aid Unsweetened Cherry (00043000955628) in 2 mM AceK in milliQ water. For the first 48 h, animals were tested for their initial preference (Pre) between solutions. Mice were then exposed to cherry only for 2 × 24 h sessions (days 3 and 5), and grape plus 0.005 g l^{-1} clozapine dihydrochloride (Hello Bio, HB6129-50mg) for 2 × 24 h sessions (days 4 and 6) for conditioning[1]. Mice were then assayed for their preference after the conditioning sessions on days 7 and 8. Initial preference is calculated as the average of days 1–2 (volume of grape solution consumed)/(total volume consumed), and post-conditioning preference is similarly calculated from days 7–8. To demonstrate that the switch is independent of the nature of the initial less-preferred stimuli, 4/8 C57BL/6J and 4/8 *Penk*-hM3Dq mice were tested with reversed flavour conditions (that is, conditioned to 0.9 g l^{-1} cherry in 1 mM AceK with clozapine).

Brief-access preference assay

C57BL/6J mice were tested for their immediate taste preferences in a short-access two-bottle preference assay[7]. Singly housed naive mice were acclimatized in new cages with access to two bottles of water overnight. Animals were then water deprived for 1h and presented with 600 mM glucose versus 600 mM MDG for 1 h. Preference for glucose was calculated as (volume of glucose consumed)/(total volume consumed).

Insulin and glucose measurements

Plasma insulin and blood glucose measurements were performed as previously described[58]. Male C57BL/6J mice were group-housed in cages with wood chip bedding. Mice were habituated to scruffing and blood draws at least twice before the experiment. On the day of sample collection, animals were subjected to a 5-h fast (food removed and transferred to clean cages) beginning at the lights-on period of the light–dark cycle (07:00). Mice were gavaged with 555 mM glucose or MDG at 2 mg kg^{-1}. Blood (~100 µl) was collected before and 15 min after gavage into a chilled heparin-coated Eppendorf tube. Glucose measurements were taken on whole blood via hand-held glucometer (OneTouch Verio). For insulin measurements, samples were run on a mouse insulin ELISA kit (Mercodia, 10-1247-01) according to the manufacturer's directions.

Retrograde labelling of vagal neurons from brainstem

C57BL/6J mice were stereotaxically injected with 50 nl of red or green fluorescent RetroBeads (Lumafluor) in the cNST or Cuneate nucleus (Paxinos stereotaxic coordinates relative to Bregma and skull surface: caudal 7.5 mm, lateral 0.9 mm, ventral 3.6–3.9 mm). Mice were euthanized 6–7 days after RetroBeads injection. Prior to analysis, the brainstem was sliced coronally to confirm accurate targeting to the cNST and Cuneate. Nodose and dorsal root ganglia (across the cervical, thoracic and lumbar segments)[59] were examined for fluorescent labelling.

Statistics

No statistical methods were used to predetermine sample size, and investigators were not blinded to group allocation. No method of randomization was used to determine how animals were allocated to experimental groups. Statistical methods used include one-way ANOVA followed by Tukey's HSD post hoc test, two-tailed *t*-test, or the two-sided Mann–Whitney *U*-test, and are indicated for all figures. All analyses were performed in MATLAB. Data are presented as mean ± s.e.m.

Reporting summary

Further information on research design is available in the Nature Research Reporting Summary linked to this paper.

Data availability

All data supporting the findings of this study are available from the corresponding author upon request.

Code availability

Custom code is available from the corresponding author.

49. Ueno, A. et al. Mouse intragastric infusion (iG) model. *Nat. Protoc.* **7**, 771–781 (2012).
50. Murray, A. J. et al. Parvalbumin-positive CA1 interneurons are required for spatial working but not for reference memory. *Nat. Neurosci.* **14**, 297–299 (2011).
51. DeNardo, L. A. et al. Temporal evolution of cortical ensembles promoting remote memory retrieval. *Nat. Neurosci.* **22**, 460–469 (2019).
52. Paxinos, G. & Franklin, K. *The Mouse Brain in Stereotaxic Coordinates* 2nd edn (Academic, 2001).
53. Lerner, T. N. et al. Intact-brain analyses reveal distinct information carried by SNc dopamine subcircuits. *Cell* **162**, 635–647 (2015).
54. Cyphert, J. M. in *Mouse Models of Allergic Disease: Methods and Protocols* (ed. Allen, I. C.) 219–227 (Humana, 2013).
55. Pnevmatikakis, E. A. & Giovannucci, A. An online algorithm for piecewise rigid motion correction of calcium imaging data. *J. Neurosci. Methods* **291**, 83–94 (2017).
56. Keemink, S. W. et al. FISSA: a neuropil decontamination toolbox for calcium imaging signals. *Sci. Rep.* **8**, 3493 (2018).
57. Friedrich, J., Zhou, P. & Paninski, L. Fast online deconvolution of calcium imaging data. *PLOS Comput. Biol.* **13**, e1005423 (2017).
58. Moriya, R., Shirakura, T., Ito, J., Mashiko, S. & Seo, T. Activation of sodium-glucose cotransporter 1 ameliorates hyperglycemia by mediating incretin secretion in mice. *Am. J. Physiol. Endocrinol. Metab.* **297**, E1358–E1365 (2009).
59. Sleigh, J. N., Weir, G. A. & Schiavo, G. A simple, step-by-step dissection protocol for the rapid isolation of mouse dorsal root ganglia. *BMC Res. Notes* **9**, 82 (2016).
60. Martin, G. *Neuroanatomy Text and Atlas* 4th edn (McGraw Hill, 2003).
61. Luo, L., Callaway, E. M. & Svoboda, K. Genetic dissection of neural circuits. *Neuron* **57**, 634–660 (2008).

Acknowledgements We thank N. Ryba for experimental suggestions and helpful comments; R. Barretto for advice on the calcium-imaging pipeline; L. Luo for the TRAP mice; S. Liberles for GPR65-Cre mice; P. Wulff for the tetanus toxin construct; A. Skowronski and C. Leduc for their assistance in performing blood glucose and insulin measurements; L. Rickman for expert help with figures; R. Lessard for earlier contributions; members of the Zuker lab for helpful discussions; and E. Sobolik, L. Hsin, Y. Zhang, A. Holguin, A. Conomikes, E. Shaw, B. McTyre and J. Li, who participated in various aspects of this work. Imaging was performed with support from the Zuckerman Institute's Cellular Imaging platform. Research reported in this publication was supported in part by the Russell Berrie Foundation program in the neurobiology of obesity (to C.S.Z. and R. Leibel). A.C.S. was supported by the MSTP program, H.-E.T. was supported by the Agency for Science, Technology and Research (A*STAR) of Singapore, and Y.G. was supported by a predoctoral fellowship from NRSA and the MSTP

program. C.S.Z. is an investigator of the Howard Hughes Medical Institute and a Senior Fellow at Janelia Farm Research Campus. Figures were generated with the help of BioRender.

Author contributions A.C.S. and H.-E.T. designed the study, carried out the experiments and analysed data, H.J. performed retrograde tracing experiments and helped with the TRAP system. M. Vignovich analysed calcium-imaging data, and helped to develop the analysis pipeline. M. Villavicencio and K.S.T. designed and characterized engineered animals and behavioural experiments. Y.G. participated in the initial phases of this study. C.S.Z. designed the study and analysed data. C.S.Z., A.C.S. and H.-E.T. wrote the paper.

Competing interests C.S.Z. is a scientific co-founder of and advisor to Kallyope. The other authors declare no competing interests.

Additional information

Supplementary information is available for this paper at https://doi.org/10.1038/s41586-020-2199-7.

Correspondence and requests for materials should be addressed to C.S.Z.

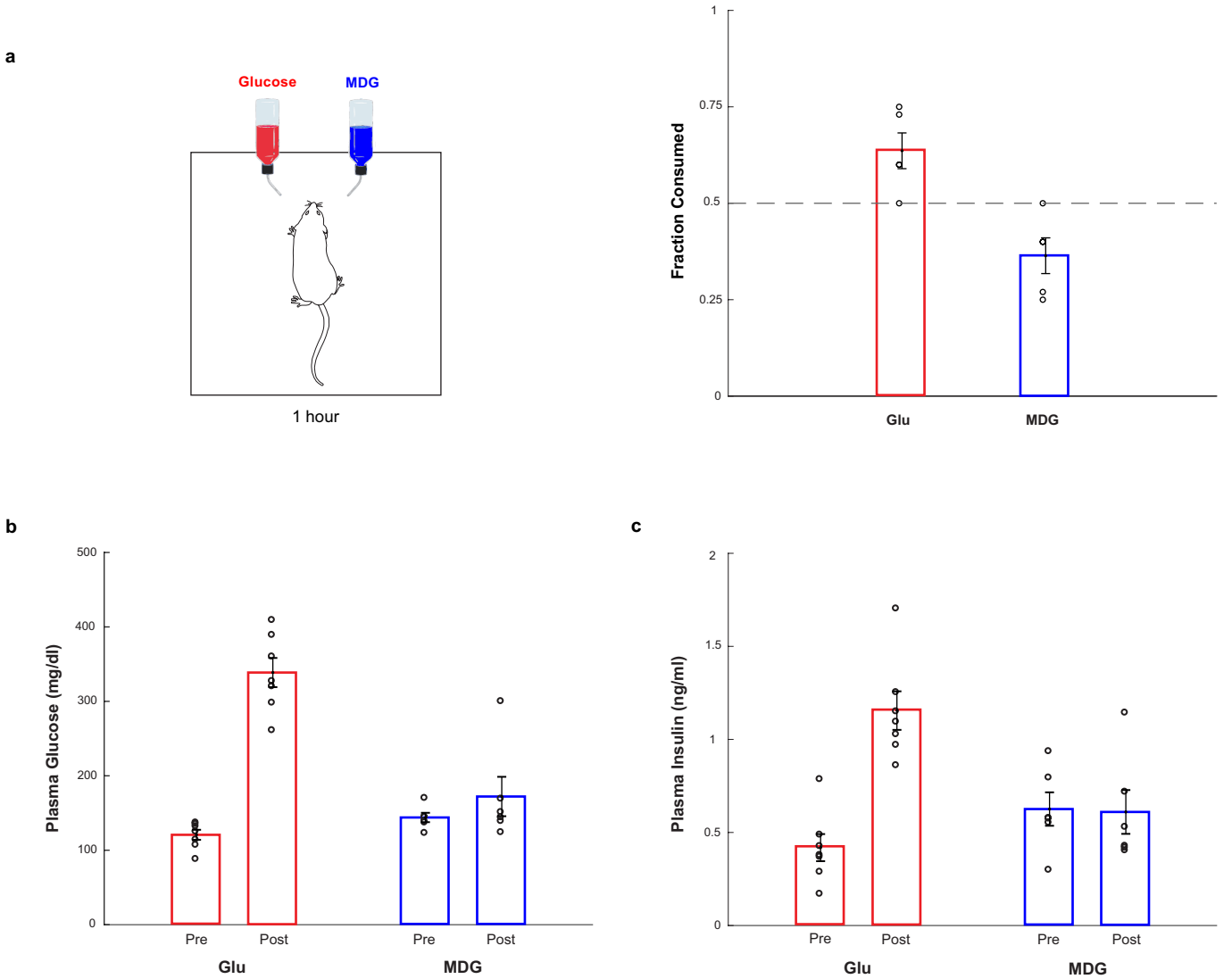

Extended Data Fig. 1 | Glucose and MDG preference. a, When mice are given a choice between 600 mM glucose or 600 mM MDG, using a brief-access (1 h) test, naive animals display a small preference for glucose over MDG ($n = 5$, two-tailed paired t-test, $P = 0.0406$), probably because MDG is slightly less sweet and thus not as attractive. Values are mean ± s.e.m. **b**, **c**, Although the non-caloric sugar analogue MDG is very effective in causing a preference switch (see Fig. 1), it does not cause increases in plasma glucose or release of insulin. Mice were gavaged with glucose or MDG, and plasma glucose and insulin levels were sampled before (Pre), and at 15 min after the gavage (Post). **b**, Plasma glucose after glucose gavage (red bars). $n = 7$, two-tailed paired t-test, $P = 4 \times 10^{-5}$. Plasma glucose after MDG gavage (blue bars). $n = 6$, two-tailed paired t-test, $P = 0.36$. **c**, Plasma insulin levels after glucose gavage (red bars). $n = 7$, two-tailed paired t-test, $P = 7 \times 10^{-6}$. Plasma insulin levels after MDG gavage (blue). $n = 6$, two-tailed paired t-test, $P = 0.94$. Values are mean ± s.e.m.

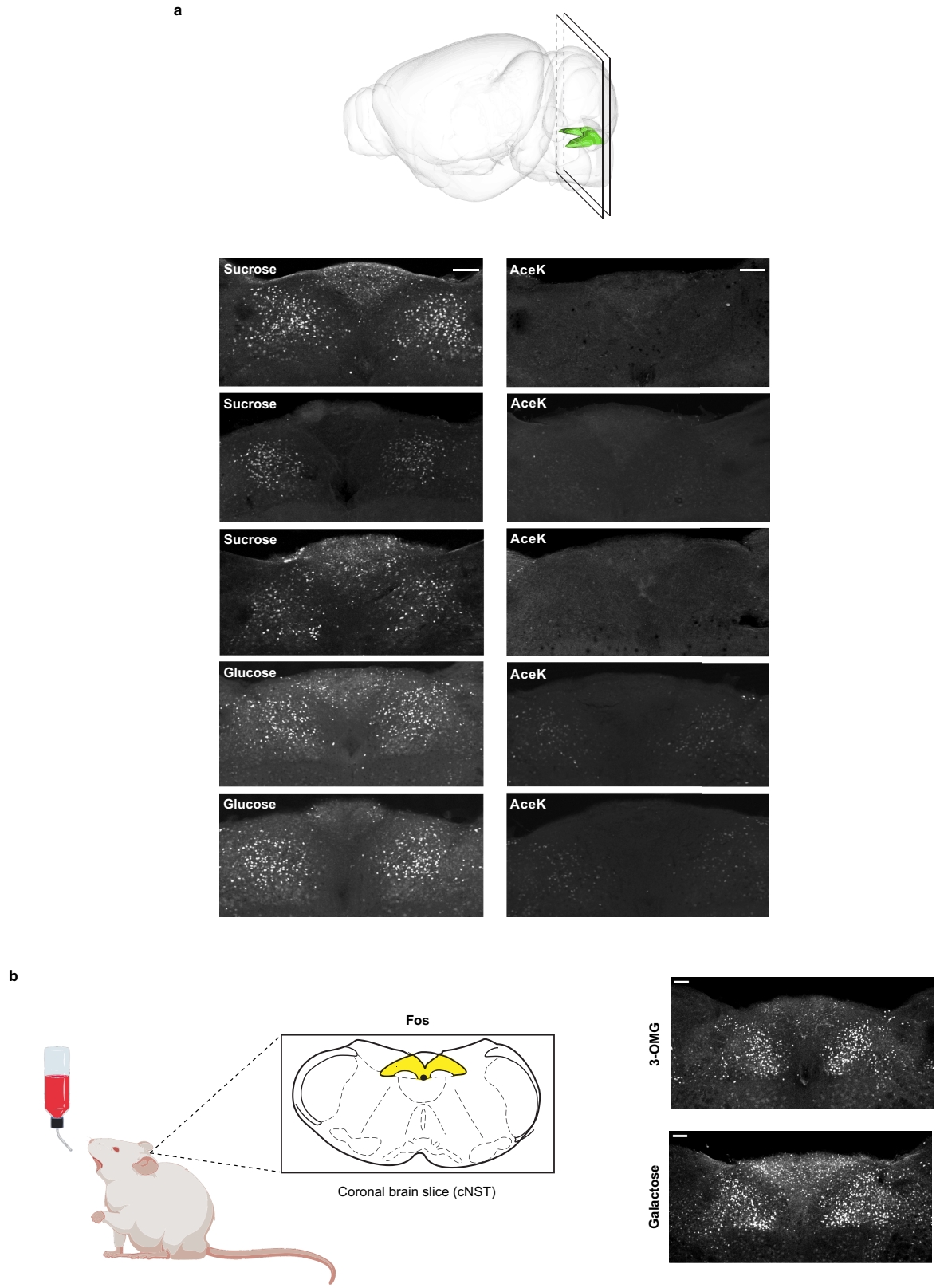

Extended Data Fig. 2 | Fos responses are robust and reliable. a, The brain diagram illustrates the position of the NST and the plane of the sectioning. Shown are cNST sections stained with Fos antibodies after exposing the animals to 90 min of 600 mM sucrose, 600 mM glucose or 30 mM AceK. Each panel is a confocal maximal projection image from Bregma −7.5 mm consisting of 3 sections 15 µm apart. Each panel (sucrose, glucose or AceK) represents a different animal, $n = 3$ independent experiments. Note the robustness of the signals across animals. See Methods for details. **b**, Mice were stimulated with 600 mM 3-OMG ($n = 6$ mice) or 600 mM galactose ($n = 3$ mice) (see also Fig. 4, Extended Data Fig. 10). Note strong Fos signals in cNST neurons, $n = 2$ independent experiments (total of 9 mice). Scale bars, 100 µm.

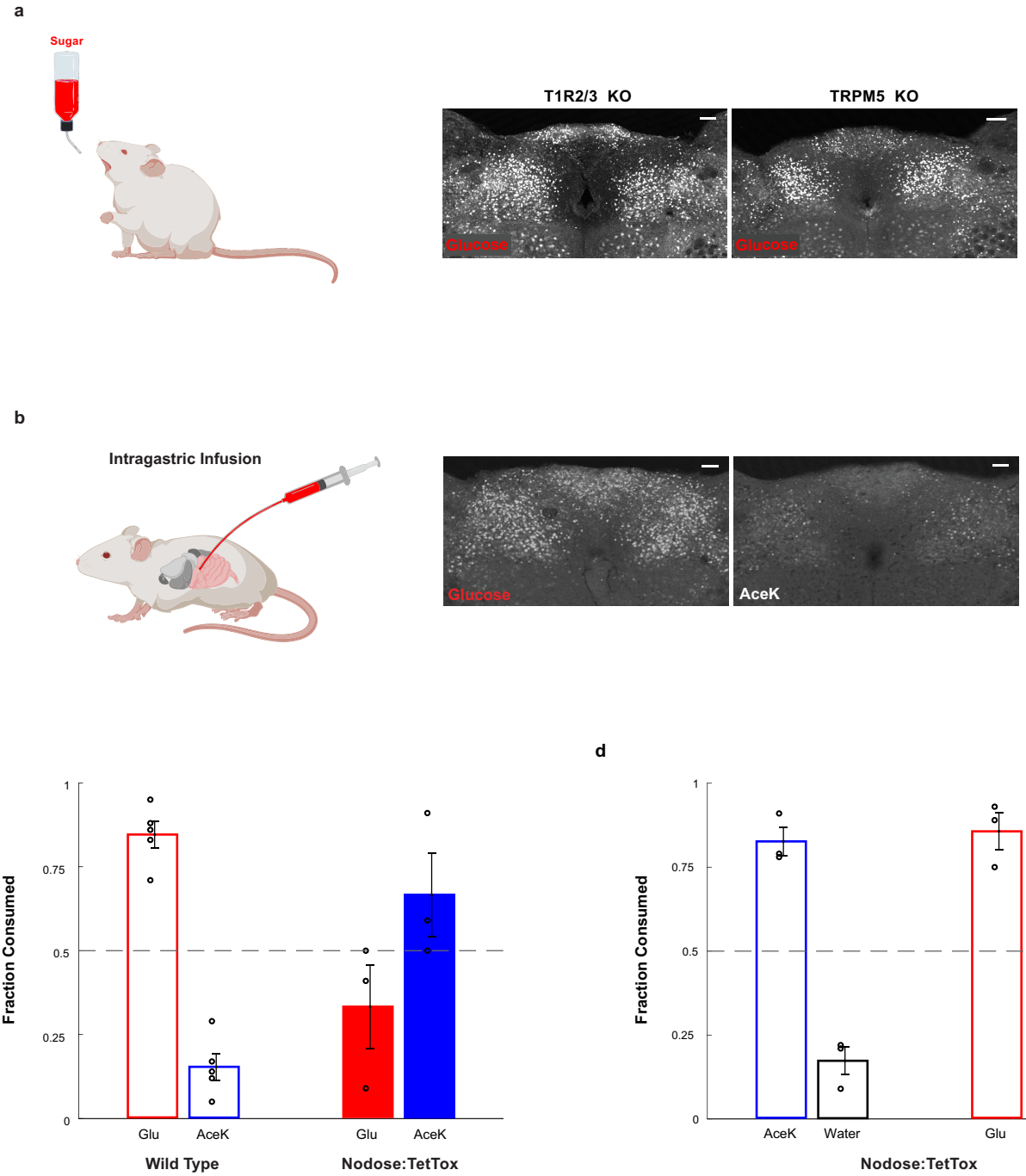

Extended Data Fig. 3 | The development of sugar preference. a, Glucose stimulates cNST neurons in mice lacking the sweet taste receptor (T1R2/3$^{-/-}$), or in mice lacking the TRPM5 ion channel (TRPM5$^{-/-}$). See Fig. 1e for quantification. T1R2/3$^{-/-}$, $n = 5$ mice, ANOVA followed by Tukey's HSD post hoc test, $P < 0.0001$; TRPM5$^{-/-}$, $n = 7$ mice, ANOVA followed by Tukey's HSD post hoc test, $P < 0.0001$. Values are mean ± s.e.m. Scale bars, 100 µm. **b**, Direct intragastric infusion of glucose, but not AceK, robustly activates the cNST. $n = 2$ independent experiments. Scale bars, 100 µm. **c**, **d**, Genetic silencing of vagal sensory neurons. **c**, Sugar-preference graphs for wild-type mice ($n = 5$ mice), demonstrating the robust development of preference for sugar versus artificial sweetener (see also Fig. 1). By contrast, silencing of the sensory neurons in the nodose ganglia, by bilateral injection of AAV-DIO-TetTox into the nodose ganglia of *Vglut2-cre* mice (see Methods), abolishes the development of sugar preference; $n = 3$ mice, two-sided Mann–Whitney *U*-test, $P = 0.035$. Values are mean ± s.e.m. **d**, However, silencing vagal sensory neurons does not impair the innate attraction to sweet solutions; shown are behavioural responses to AceK versus water, and glucose versus water ($n = 3$ animals, preference index for AceK = 0.82, preference index for glucose = 0.85). Values are mean ± s.e.m.

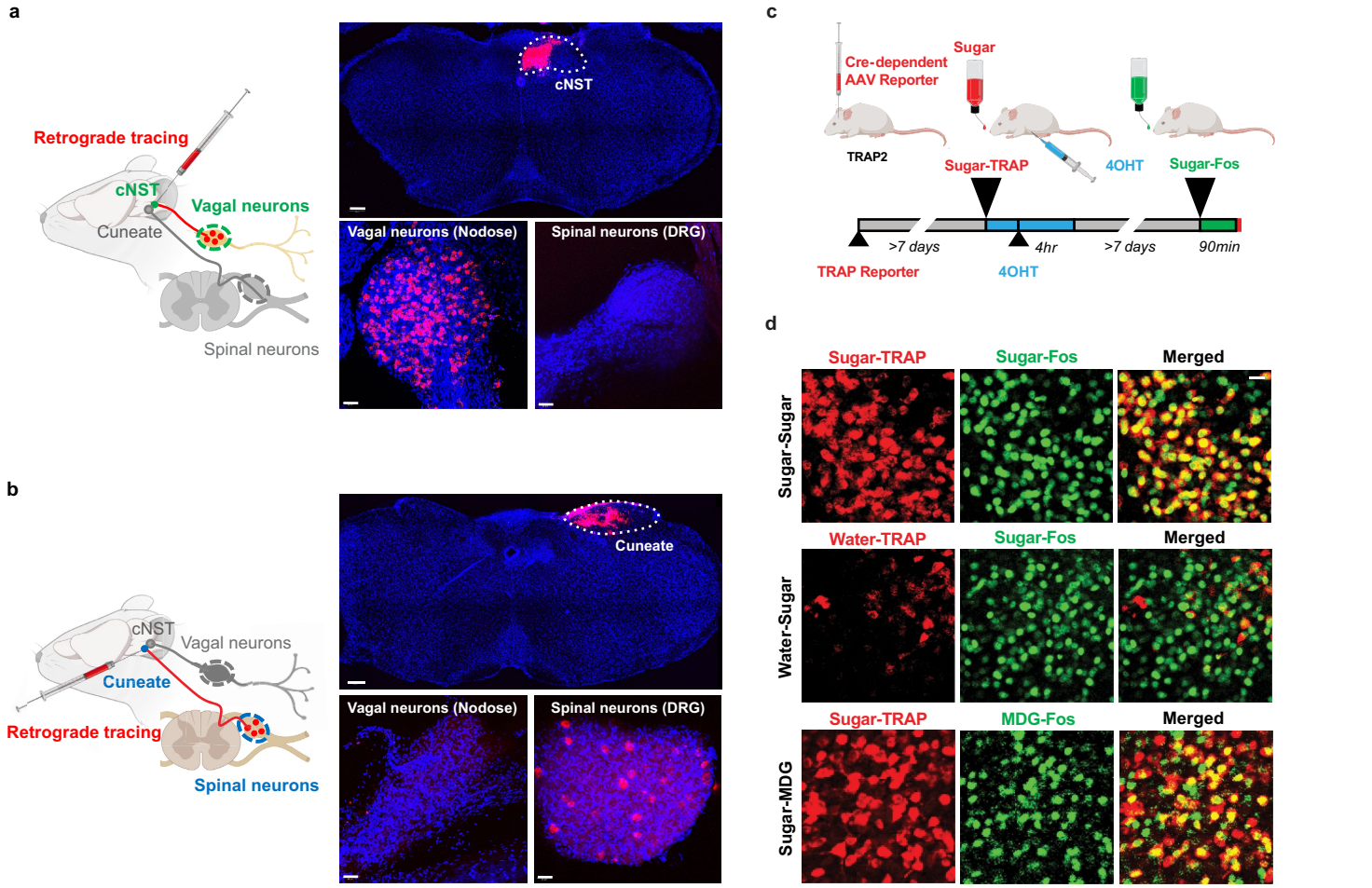

Extended Data Fig. 4 | Retrograde labelling from cNST. a, A fluorescent retrograde tracer (red RetroBeads, Lumafluor) was stereotactically injected into the cNST to label its inputs. The nodose ganglia and dorsal root ganglia were checked for transfer of the fluorescent label after 6–7 days. The nodose ganglion (vagal neurons), but not the dorsal root ganglion (spinal neurons), was robustly labelled[60]. $n = 2$ independent experiments. **b**, RetroBeads were also injected into the cuneate nucleus, a brainstem area near but distinct from the cNST. Vagal neurons were not labelled. By contrast, note robust labelling of spinal neurons ($n = 2$ independent experiments). Nuclei were counterstained with DAPI (blue). Scale bars, 200 µm (Brainstem), 50 µm (nodose, DRG). **c**, Validation of TRAPing procedure to confirm that the sugar-activated cNST neurons marked by the expression of Fos are the same as the ones labelled by Cre recombinase in the genetic TRAPing experiments. We genetically labelled the sugar-induced TRAPed neurons with a Cre-dependent fluorescent reporter[61], and then performed a second cycle of sugar stimulation followed by Fos antibody labelling. **d**, Top, neurons labelled by the Cre-dependent reporter after sugar TRAPing ('sugar-TRAP', pseudocoloured red) are the same as those labelled by Fos after a second cycle of sugar stimulation ('sugar-Fos', green; see Methods and text for details), >80% of Sugar-Fos neurons are also sugar-TRAP positive ($n = 7$ animals). Middle, note that the few neurons labelled after water-TRAP in response to water do not overlap with those labelled with Fos antibodies after sugar stimulation. Bottom, the sugar-TRAP neurons are also activated by the non-caloric sugar analogue MDG; >80% of MDG-Fos are sugar-TRAP positive. Scale bar, 20 µm.

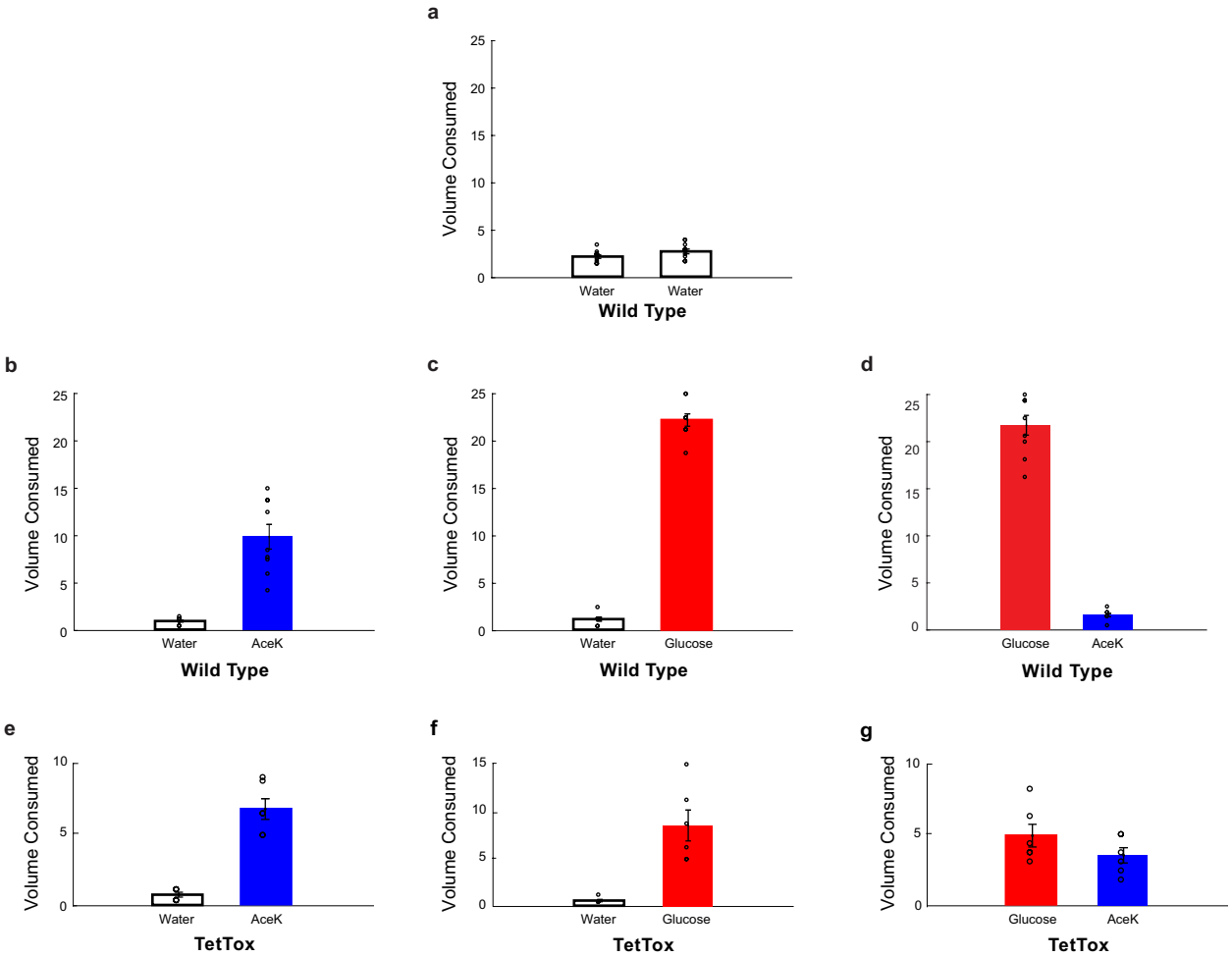

Extended Data Fig. 5 | Mice with a silenced sugar-preference circuit behave as normal mice, drinking artificial sweeteners. a, A normal, non-thirsty mouse drinks about 5 ml of water during a 24-h window. $n = 11$ mice. Values are mean ± s.e.m. **b**, If presented with a sweet option (but not sugar, so as to not create a preference) they show a small but significant increase in total volume consumed, but now most of the total consumption is from the sweet choice rather than water ($n = 9$ animals, two-tailed paired t-test, $P = 1 \times 10^{-4}$). Values are mean ± s.e.m. **c**, By contrast, if the options are water versus sugar, so that it creates a preference, they massively increase total volume consumed, and nearly all is from the sugar solution ($n = 9$ animals, two-tailed paired t-test, $P = 3 \times 10^{-10}$). Values are mean ± s.e.m. **d**, As expected, wild-type controls develop a strong preference for sugar versus AceK ($n = 9$ animals, two-tailed paired t-test, $P = 3 \times 10^{-8}$). Values are mean ± s.e.m. **e**, **f**, Mice with the preference circuit silenced behave as control animals presented with a sweet, non-preference creating choice (compare **e**, **f** with **b**) ($n = 6$ mice, two-tailed paired t-test, $P = 6 \times 10^{-4}$ for AceK, $P = 4 \times 10^{-3}$ for glucose). Values are mean ± s.e.m. **g**, Silenced animals consumed nearly equal volumes of sugar and artificial sweetener ($n = 6$ animals, two-tailed paired t-test, $P = 0.1$). Values are mean ± s.e.m.

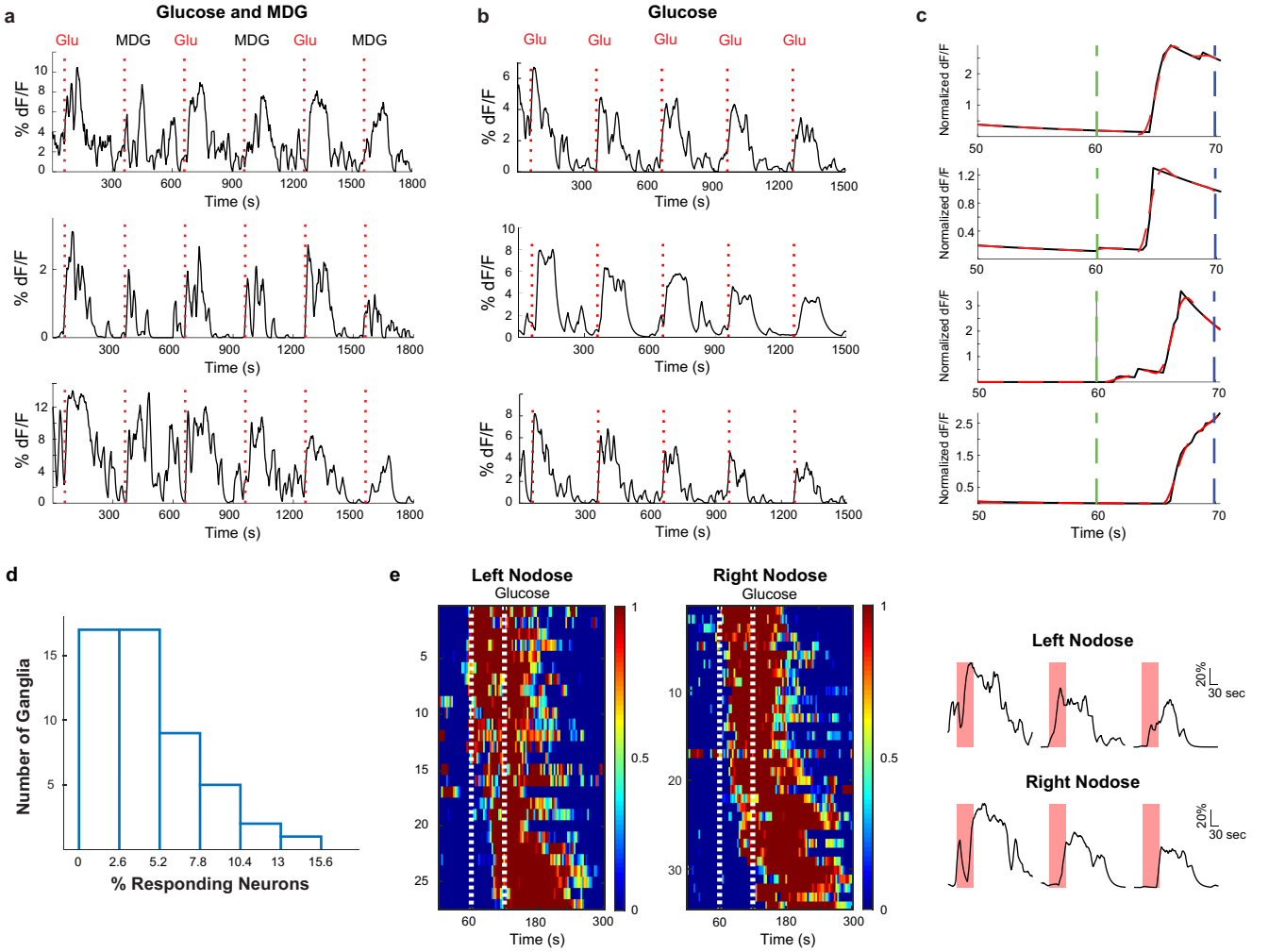

Extended Data Fig. 6 | Vagal-neuron responses to sugar and MDG are highly reproducible and timed-locked to the stimulus. a, Shown are vagal-neuron responses to 6 consecutive 10-s intestinal stimuli of alternating trials with 500 mM glucose and 500 mM MDG (stimulus delivery and timings are as described in the Methods). Each of the sample traces depicts the response from a different neuron. **b**, Shown are vagal-neuron responses to 5 consecutive 10-s intestinal stimuli with 500 mM glucose (stimulus delivery and timings are as described in the Methods). Each of the sample traces shows the response from a different neuron. **c**, Expanded time scale of responses to the 10-s 500 mM glucose stimulus from 10 s before to 10 s after termination of the stimulus. The green dashed lines indicate the initiation of the stimulus, and the blue dashed lines denote termination of the 10-s stimulus. Calcium responses are shown in solid black and exponential fits to the response latency and kinetics are shown in red. Note responses time-locked to stimulus delivery; the top two traces depict two cells from two different mice in response to glucose, and the bottom two traces depict two cells from two different mice in response to MDG; latencies varied between 3 and 6 s, and were within the 10-s stimulation window. Some cells exhibited longer latencies (see for example, heat maps in Fig. 4, Extended Data Fig. 8). We believe the cells with longer response latencies may represent intestinal glucose responders located farther down the intestinal segment, and thus would be expected to demonstrate longer latencies[37]. **d**, On average, approximately 5% of vagal neurons respond reliably to a 10-s 500 mM glucose stimulus. The histogram shows the percentage of GCaMP-expressing vagal neurons responding to the 10-s glucose stimulus. Average = 4.6 ± 0.05% (n = 4,803 neurons from 51 ganglia, mean ± s.e.m.). **e**, Recent findings[25] have suggested that appetitive behavioural responses are elicited through stimulation of vagal terminals originating from the right nodose ganglion. Shown are heat maps depicting z-score normalized average calcium responses of individual ganglion neurons after a 60-s pulse of 500 mM glucose. We observe no differences in responses to intestinal glucose from either the left or right vagal ganglia. Also shown are example traces from different neurons from the left and right Nodose ganglion; red bars indicate the 60-s stimulus; scale bars indicate percentage maximal response.

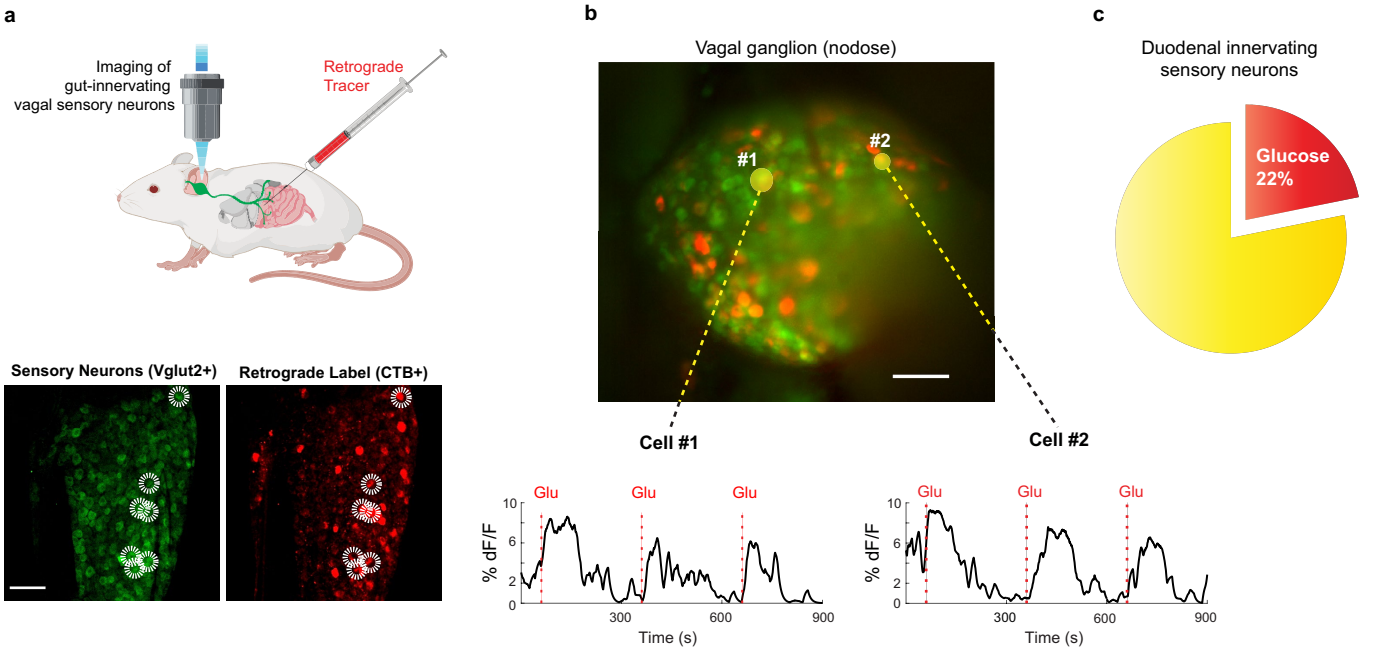

Extended Data Fig. 7 | Vagal neurons innervating duodenal segment sense sugar. a, Top, schematic of retrograde tracing experiment. Fluorescently conjugated CTB[38] was injected into the proximal duodenum to back fill and label the cell bodies of duodenum-projecting vagal neurons (*z*-projection of $n = 22$ confocal planes from a representative ganglion, see Methods for details). The two bottom panels show a sample retrogradely labelled ganglion with sensory neurons (*Vglut2-cre* driving the GCaMP reporter) marked in green (left) and those labelled by CTB marked by red fluorescence (right). Double-positive neurons are highlighted by the white circles. Scale bar, 100 µm. **b**, Representative field of a vagal imaging session showing the overlay of CTB and GCaMP. The two yellow circled neurons (denoted as #1 and #2) were labelled by retrogradely applied CTB in the duodenal segment, and exhibited strong responses to glucose ($n = 16$ ganglia from 10 mice). Scale bar, 100 µm. **c**, A total of 12 out of 55 double-positive neurons responded to the 10-s glucose stimulus (see Extended Data Fig. 6d for a comparison with uninjected animals). $n = 16$ ganglia from 10 mice. Note the substantial enrichment in the number of responders when pre-tagged by retrograde labelling: ~20% in the duodenal tagged versus 4–5% in the whole population.

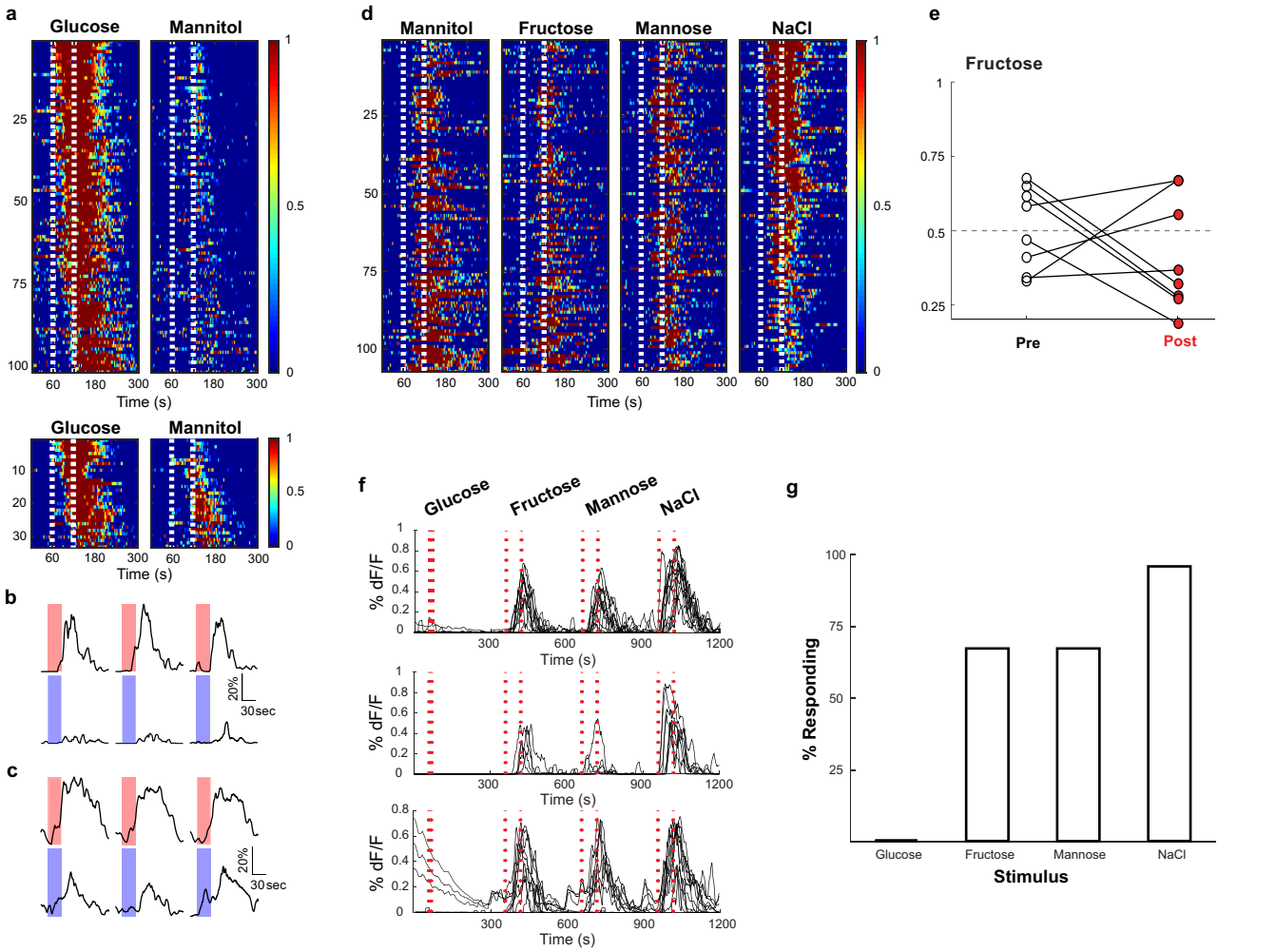

Extended Data Fig. 8 | Glucose responders are not sensing osmolarity. Williams et al.[24] identified vagal neurons that indiscriminately responded to high concentrations of several stimuli delivered in very large stimulus volume for hundreds of seconds. We believe these responses, largely independent of the quality of the stimulus, are intestinal osmolarity signals. **a**, Shown are heat maps summarizing responses to interleaved 60-s stimuli of 500 mM glucose and 500 mM mannitol. Each row represents the average activity of a single cell during three interspersed exposures to the stimulus. Stimulus window is indicated by the dashed white lines. Of 134 neurons that responded to intestinal application of 500 mM glucose for 60 s, 101 did not exhibit statistically significant responses to mannitol (top). However, 33 (~25%) showed responses to both 500 mM glucose and 500 mM mannitol (bottom). $n = 5$ mice. When the intestinal stimulus consisted of a short pulse (that is, 10 s; 33 µl volume) no responses were detected to 500 mM mannitol (data not shown). **b**, Sample traces (three trials each) of a neuron responding to glucose (red) but not mannitol (blue). **c**, Sample traces (three trials each) of a neuron responding to glucose and mannitol. Scale bars indicate percentage maximal response. **d**, Heat maps showing responses to a 60-s stimuli of 1 M mannitol, 1 M fructose, 1 M mannose and 1 M NaCl. Note that the same cells respond indiscriminately to the various stimulus ($n = 4$ mice). **e**, The graph shows preference plots for fructose versus AceK ($n = 8$ mice, two-tailed paired t-test, $P = 0.27$). Note that fructose, a caloric sugar, does not create preference, but activates osmolarity responses. **f**, Williams et al.[24] suggest that GPR65-expressing vagal neurons function as the nutrient sensors. We generated mice in which GCaMP6s expression was targeted to GPR65-expressing vagal neurons and examined their responses to a 10-s stimulus of 500 mM glucose or osmolarity signals (that is, 1 M each of fructose, mannose and NaCl for 60 s). Shown are normalized responses of from three different mice to the four stimuli; each trace represents a different responding neuron. Note that 500 mM glucose for 10 s does not activate GPR65 neurons. By contrast, they are activated by 60-s pulse of 1 M fructose, mannose and NaCl (see also Fig. 4). **g**, Summary histogram of GPR65 tuning profile to 10 s 500 mM glucose, and 60 s 1 M fructose, 60 s 1 M mannose and 60 s 1 M NaCl; $n = 4$ mice.

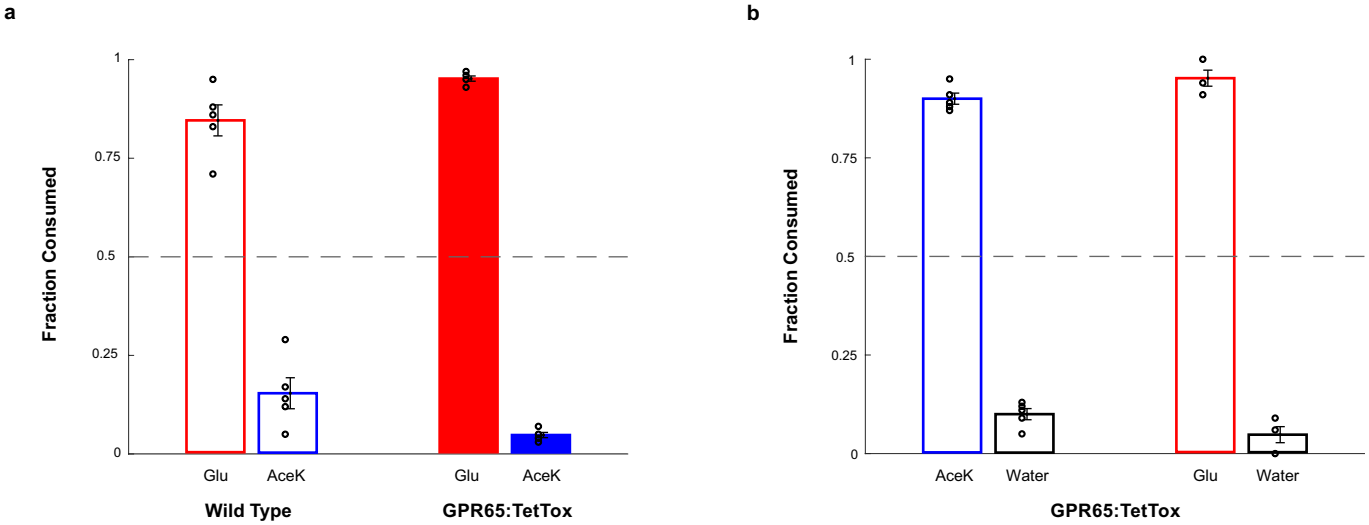

Extended Data Fig. 9 | Genetic silencing of GPR65 neurons does not affect the development of sugar preference. a, Global silencing of the GPR65 neurons was achieved by generating GPR65-IRES-Cre; R26-TeNT double transgenic animals expressing TetTox in GPR65 neurons. Sugar-preference graphs demonstrating the robust development of preference for sugar versus artificial sweetener for both wild-type ($n = 5$ mice, two-tailed paired t-test, $P = 0.0047$) and GPR65:TetTox mice ($n = 5$ mice, two-tailed paired t-test, $P = 0.0033$). The wild-type controls shown here are the same mice used in Extended Data Fig. 3c, as both sets of silencing experiments were carried out as part of the same series of studies. Values are mean ± s.e.m. **b**, Silencing of GPR65 neurons does not impair the innate attraction to sweet solutions. Shown are behavioural responses to AceK versus water and glucose versus water ($n = 5$, two-tailed paired t-test, $P = 0.0040$ for consumed volumes of AceK versus water, $P = 0.0023$ for consumed volumes of glucose versus water). Values are mean ± s.e.m.

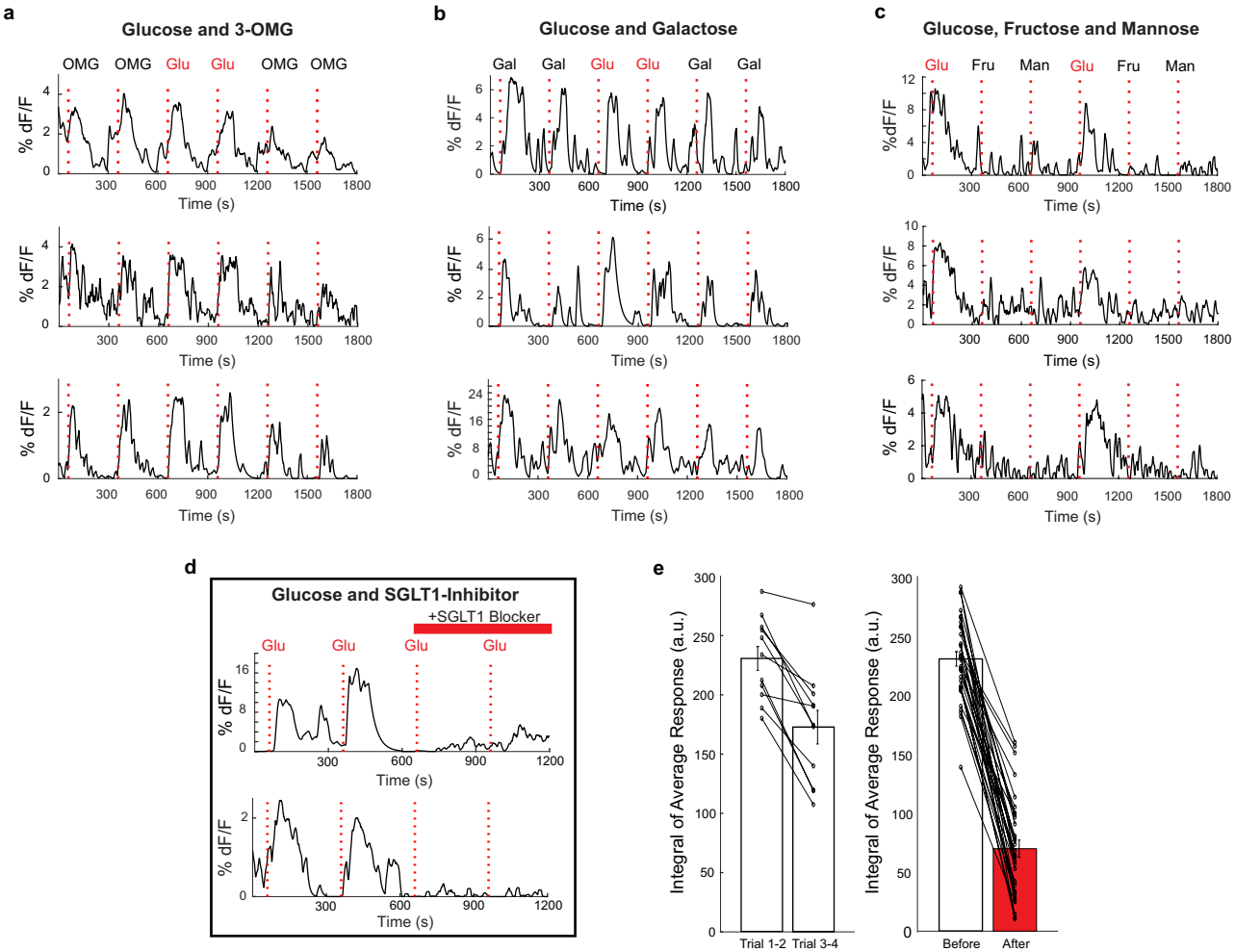

Extended Data Fig. 10 | Vagal neurons responding to intestinal glucose are also activated by SGLT1 agonists. a, Traces of vagal neurons responding to a 10-s pulse of 500 mM intestinal glucose, also challenged with a 10-s pulse of 500 mM 3-OMG. Shown are sample neurons from 2 animals. **b**, Traces of vagal neurons responding to a 10-s pulse of 500 mM intestinal glucose, also challenged with a 10-s pulse of 500 mM galactose. Shown are sample neurons from two animals for expanded time scales (from Fig. 4d). **c**, Traces of vagal neurons responding to a 10-s pulse of 500 mM intestinal glucose, also challenged with a 10-s pulse of 500 mM fructose and 500 mM mannose. Shown are sample neurons from three mice. **d**, Traces of vagal neurons responding to two consecutive 10-s pulses of 500 mM intestinal glucose, before and after treating the intestinal segment with 8 mM phlorizin for 5 min. Note the loss of responses. **e**, Because responses, in general, show some decay during the time of the experiment (in part due to desensitizing and bleaching of the fluorescent signals), we also analysed the average decay of corresponding glucose responses in the absence of any blocker. The graphs compare the loss of responses during normal decay, and in response to the blocker. For normal decay (left), $n = 11$ neurons, Pre = 230.8 arbitrary units (a.u.), Post = 172.8 a.u.; for blocker (right), $n = 31$ neurons, Pre = 229.7 a.u., Post = 67.0 a.u. All values are mean ± s.e.m. Scale indicates average integral of the responses to the two trials before and after inhibition.

nature research

Corresponding author(s): Charles S. Zuker

Last updated by author(s): Feb 9, 2020

Reporting Summary

Nature Research wishes to improve the reproducibility of the work that we publish. This form provides structure for consistency and transparency in reporting. For further information on Nature Research policies, see Authors & Referees and the Editorial Policy Checklist.

Statistics

For all statistical analyses, confirm that the following items are present in the figure legend, table legend, main text, or Methods section.

n/a	Confirmed	
☐	☒	The exact sample size (*n*) for each experimental group/condition, given as a discrete number and unit of measurement
☐	☒	A statement on whether measurements were taken from distinct samples or whether the same sample was measured repeatedly
☐	☒	The statistical test(s) used AND whether they are one- or two-sided *Only common tests should be described solely by name; describe more complex techniques in the Methods section.*
☒	☐	A description of all covariates tested
☒	☐	A description of any assumptions or corrections, such as tests of normality and adjustment for multiple comparisons
☐	☒	A full description of the statistical parameters including central tendency (e.g. means) or other basic estimates (e.g. regression coefficient) AND variation (e.g. standard deviation) or associated estimates of uncertainty (e.g. confidence intervals)
☐	☒	For null hypothesis testing, the test statistic (e.g. *F*, *t*, *r*) with confidence intervals, effect sizes, degrees of freedom and *P* value noted *Give P values as exact values whenever suitable.*
☒	☐	For Bayesian analysis, information on the choice of priors and Markov chain Monte Carlo settings
☒	☐	For hierarchical and complex designs, identification of the appropriate level for tests and full reporting of outcomes
☒	☐	Estimates of effect sizes (e.g. Cohen's *d*, Pearson's *r*), indicating how they were calculated

Our web collection on statistics for biologists contains articles on many of the points above.

Software and code

Policy information about availability of computer code

Data collection	Tucker-Davis Technologies Synapse (Version 90-39473P), MicroManager (Version 1.4), Olympus Fluoview (FV10), Arduino IDE (Version 1.8.10), MathWorks Matlab (R2019a, R2019b)
Data analysis	MathWorks Matlab (R2019b), FIJI (Version 1.52p)

For manuscripts utilizing custom algorithms or software that are central to the research but not yet described in published literature, software must be made available to editors/reviewers. We strongly encourage code deposition in a community repository (e.g. GitHub). See the Nature Research guidelines for submitting code & software for further information.

Data

Policy information about availability of data

All manuscripts must include a data availability statement. This statement should provide the following information, where applicable:

- Accession codes, unique identifiers, or web links for publicly available datasets
- A list of figures that have associated raw data
- A description of any restrictions on data availability

All data supporting the findings of this study are available upon reasonable request.

Field-specific reporting

Please select the one below that is the best fit for your research. If you are not sure, read the appropriate sections before making your selection.

☒ Life sciences ☐ Behavioural & social sciences ☐ Ecological, evolutionary & environmental sciences

Life sciences study design

All studies must disclose on these points even when the disclosure is negative.

Sample size	Sample size was determined based similar studies in the literature and our experience. No statistical method was used to determine the sample size prior to the study.
Data exclusions	Animals in which post-hoc histological examination showed that viral targeting or the position of implanted fiber were in the incorrect location were excluded from analysis. This exclusion criteria was predetermined.
Replication	We performed multiple independent experiments as noted in the figure legends. Results were reproducible.
Randomization	Stimuli order was random, otherwise in situations as described in the manuscript where no randomization was used, the stimuli were interspersed and repeated among trials.
Blinding	Investigators were not blinded to group allocation, as data analysis was performed automatically with the same scripts executed for each experimental group.

Reporting for specific materials, systems and methods

We require information from authors about some types of materials, experimental systems and methods used in many studies. Here, indicate whether each material, system or method listed is relevant to your study. If you are not sure if a list item applies to your research, read the appropriate section before selecting a response.

Materials & experimental systems

n/a	Involved in the study
☐	☒ Antibodies
☒	☐ Eukaryotic cell lines
☒	☐ Palaeontology
☐	☒ Animals and other organisms
☒	☐ Human research participants
☒	☐ Clinical data

Methods

n/a	Involved in the study
☒	☐ ChIP-seq
☒	☐ Flow cytometry
☒	☐ MRI-based neuroimaging

Antibodies

Antibodies used	anti c-Fos (Santa Cruz, SC52G, K1715, Goat, 1:500), anti c-Fos (Synaptic Systems, 226004, Guinea Pig, 1:5000)
Validation	Both antibodies has been validated extensively, e.g. by immuno-staining on mouse brain sections (Choi, et al. Cell, 146, 1004-1015, (2011), Song, et al. Science advances, 52: eaat3210, (2019)).

Animals and other organisms

Policy information about studies involving animals; ARRIVE guidelines recommended for reporting animal research

Laboratory animals	Adult animals 6-24 weeks of age and from both genders were used in experiments. C57BL/6J (JAX #000664), ArcCreER (TRAP, JAX #021881), TRAP2 (JAX #030323), TRPM5 KO (JAX #013068), T1R2/T1R3 double KO (generated in house, JAX #013065/013066), Ai96 (JAX #028866), Vglut2-IRES-Cre (JAX #028863), Gpr65-IRES-Cre (JAX #029282), Penk-IRES2-Cre (JAX #025112), Ai75D (JAX #025106), R26-TeNT (MGI #3839913).
Wild animals	No wild animals were used.
Field-collected samples	No field-collected samples were used.
Ethics oversight	All procedures were carried out in accordance with the US National Institutes of Health (NIH) guidelines for the care and use of laboratory animals, and were approved by the Institutional Animal Care and Use Committee at Columbia University.

Note that full information on the approval of the study protocol must also be provided in the manuscript.